ARNOL′D TONGUES ARISING FROM A GRAZING-SLIDING BIFURCATION OF A PIECEWISE-SMOOTH SYSTEM

RÓBERT SZALAI* AND HINKE M. OSINGA*

Abstract. The Neĭmark-Sacker bifurcation, or Hopf bifurcation for maps, is a well-known bifurcation for smooth dynamical systems. At a Neĭmark-Sacker bifurcation a periodic orbit loses stability and, except for certain so-called strong resonances, an invariant torus is born; the dynamics on the torus can be either quasi-periodic or phase locked, which is organized by Arnol′d tongues in parameter space. Inside the Arnol′d tongues phase-locked periodic orbits exist that disappear in saddle-node bifurcations on the tongue boundaries. In this paper we investigate whether a piecewise-smooth system with sliding regions may exhibit an equivalent of the Neĭmark-Sacker bifurcation. The vector field defining such a system changes from one region in phase space to the next and the dividing so-called switching surface contains a sliding region if the vector fields on both sides point towards the switching surface. The existence of a sliding region has a superstabilizing effect on periodic orbits interacting with it. In particular, the associated Poincaré map is non-invertible. We consider the *grazing-sliding bifurcation* at which a periodic orbit becomes tangent to the sliding region. We provide conditions under which the grazing-sliding bifurcation can be thought of as a Neĭmark-Sacker bifurcation. We give a normal form of the Poincaré map derived at the grazing-sliding bifurcation and show that the resonances are again organized in Arnol′d tongues. The associated periodic orbits typically bifurcate in border-collision bifurcations that can lead to dynamics that is more complicated than simple quasi-periodic motion. Interestingly, the Arnol′d tongues of piecewise-smooth systems look like strings of connected sausages and the tongues close at double border-collision points. Since in most models of physical systems non-smoothness is a simplifying approximation, we relate our results to regularized systems. As one expects, the phase-locked solutions deform into smooth orbits that, in a neighborhood of the Neĭmark-Sacker bifurcation, lie on a smooth torus. The deformation of the Arnol′d tongues is more complicated; in contrast to the standard scenario, we find several coexisting pairs of periodic orbits near the points where the Arnol′d tongues close in the piecewise-smooth system. Nevertheless, the unfolding near the double border-collision points is also predicted as a typical scenario for nondegenerate smooth systems.

AMS subject classifications. 70K30, 70K45, 70K50, 70K70, 37E05, 37G15

1. Introduction. Piecewise-smooth dynamical systems often arise when modeling, say, mechanical systems that involve Coulomb friction, or electrical circuits with relays and switches, as well as in many other areas of applications [10, 44, 46]. We focus here on systems of piecewise-smooth vector fields that have discontinuous right-hand sides, that is, they are of the form

$$\dot{\mathbf{x}} = \begin{cases} \mathbf{f}_1(\mathbf{x}) & \text{if} \quad h(\mathbf{x}) < 0, \\ \mathbf{f}_2(\mathbf{x}) & \text{if} \quad h(\mathbf{x}) > 0, \end{cases} \tag{1.1}$$

where $\mathbf{f}_1, \mathbf{f}_2 \in C^r(\mathbb{R}^n, \mathbb{R}^n)$ are two different right-hand sides and $h \in C^r(\mathbb{R}^n, \mathbb{R})$ is the event function. The velocity functions $\mathbf{f}_1$ and $\mathbf{f}_2$ are discontinuous along the $(n-1)$-dimensional manifold $\Sigma = \{\mathbf{x} \in \mathbb{R}^n : h(\mathbf{x}) = 0\}$, called the switching surface. We define the flow of (1.1) on Σ according to Filippov [17] in the following way. We consider the product $(\nabla h(\mathbf{x}) \cdot \mathbf{f}_1(\mathbf{x}))(\nabla h(\mathbf{x}) \cdot \mathbf{f}_2(\mathbf{x}))$ on Σ, that is, we compare the directions of the two vector fields with the normal $\nabla h(\mathbf{x})$ of Σ at a point $\mathbf{x} \in \Sigma$. If both vector fields point in the same direction as $\nabla h(\mathbf{x})$, that is, the product is positive, then one velocity vector points into the region outside its domain of definition and the other points inside its domain of definition. In this case, a trajectory just

*Bristol Centre for Applied Nonlinear Mathematics, Department of Engineering Mathematics, University of Bristol, Bristol BS8 1TR, United Kingdom (H.M.Osinga@bristol.ac.uk).

RS was supported by grant EP/C544048/1 from the Engineering and Physical Sciences Research Council (EPSRC) and HMO by an EPSRC Advanced Research Fellowship and an IGERT grant.

passes through Σ and there is no need to define additional dynamics. However, if $(\nabla h(\mathbf{x}) \cdot \mathbf{f}_1(\mathbf{x}))(\nabla h(\mathbf{x}) \cdot \mathbf{f}_2(\mathbf{x})) \leq 0$ then the vector fields point in opposite directions with respect to Σ. In particular when both vectors point into the regions outside their respective domains of definition, the flow is pushed towards Σ on both sides and we must make this part of Σ invariant under the dynamics. Such regions on Σ with $(\nabla h(\mathbf{x}) \cdot \mathbf{f}_1(\mathbf{x}))(\nabla h(\mathbf{x}) \cdot \mathbf{f}_2(\mathbf{x})) \leq 0$ are called sliding regions. Filippov [17] describes the dynamics on Σ in a sliding region by the sliding vector field

$$\dot{\mathbf{x}} = \lambda \mathbf{f}_1(\mathbf{x}) + (1-\lambda)\mathbf{f}_2(\mathbf{x}),$$

where λ is the unique solution to the invariance condition $\nabla h(\mathbf{x}) \cdot (\lambda \mathbf{f}_1(\mathbf{x}) + (1-\lambda)\mathbf{f}_2(\mathbf{x})) = 0$. Hence, the velocity vector is the linear combination of the two velocity vectors $\mathbf{f}_1(\mathbf{x})$ and $\mathbf{f}_2(\mathbf{x})$ such that the direction of the flow is tangent to Σ. There are different ways of dealing with the sliding regions [6], but in most cases the definition of Filippov agrees with the physics observed in experiments.

The presence of the switching surface Σ in Filippov systems induces many bifurcations in addition to what is known for smooth systems [10, 46]. Moreover, the bifurcation analysis strongly depends on the system dimensions and the number and relative location of the switching surfaces [10, 21, 25, 41]. We focus specifically on a possible equivalent of the Neĭmark-Sacker bifurcation.

The Neĭmark-Sacker bifurcation of a periodic orbit of a smooth vector field is well known [24]. The periodic orbit loses stability as a pair of Floquet multipliers moves through the complex unit circle. By considering the Poincaré map on a (local) section transverse to the periodic orbit, this corresponds to a Hopf bifurcation for a diffeomorphism, where a pair of complex conjugate eigenvalues of the corresponding fixed point of the Poincaré map moves through the complex unit circle. Unless the argument μ of the Floquet multipliers (or eigenvalues) is of the form $\frac{p}{q}$ with $q \leq 4$, which are called the strong resonances, the Neĭmark-Sacker bifurcation gives rise to an invariant torus (an invariant circle for the map) [40]. The argument μ determines the dynamics on the torus, which can be either quasi-periodic or phase locked. In a two-parameter space one would have a curve of Neĭmark-Sacker bifurcations and each point on it corresponds to a different value of μ. Off this curve emanate Arnol′d tongues, also called resonance tongues, inside of which the dynamics is phase locked. The tongue tips start on the Neĭmark-Sacker curve at rational values of $\mu = \frac{p}{q}$ and widen to a two-dimensional resonance region containing a pair of periodic orbits with rotation number p/q that disappear in saddle-node bifurcations along the tongue boundary. Points on the Neĭmark-Sacker curve with μ irrational do not have Arnol′d tongues associated with them. From such points codimension-one curves emanate along which the dynamics is quasi-periodic with irrational rotation number μ.

The classical image of the Arnol′d tongue scenario is provided by a kind of normal form called the Arnol′d circle map [1]. This map describes the dynamics on an invariant circle, where the tongue tips emanate from one of the parameter axes, but this line does not actually correspond to a Neĭmark-Sacker bifurcation. It is perhaps less well known that the Arnol′d circle map only provides part of the story on Arnol′d tongues. For example, there are many additional bifurcations happening inside the tongues that typically destroy the invariant torus [5, 32]. In more general systems, the Neĭmark-Sacker curve typically contains so-called Chenciner points [8] where the bifurcation changes from supercritical to subcritical. At such points the orientation of the tips of the Arnol′d tongues changes, and tongues tend to bend back and cross the Neĭmark-Sacker curve again at nonzero width. This behavior can be understood using

singularity theory by viewing the Arnol′d tongues as projections of regular surfaces in a higher-dimensional space; see [26, 27] and more recently [2]. We also refer to [34, 35] for more details, applications and computational methods.

There is no systematic theory of a Neĭmark-Sacker-like bifurcation for piecewise-smooth systems. As early as 1987, Yang and Hao [45] studied a piecewise-linear version of the Arnol′d circle map and found that the structure of the Arnol′d tongues in a two-parameter plane is very similar to the classical Arnol′d circle map. However, while the Arnol′d tongues for the classical circle map grow wider as one moves further away from the tongue tip, the Arnol′d tongues of the piecewise-linear circle map have nonzero width at specific points in the parameter space. Yang and Hao called such point shrinking points and likened the Arnol′d tongues to strings of sausages. An exhaustive analysis of piecewise-linear circle maps can be found in Campbell et al. [7], where the close-up of the resonance tongues is associated with a linear circle map of unit slope.

More recent studies consider Arnol′d tongues for Filippov systems of the form (1.1) that do not exhibit sliding, that is, $(\nabla h(\mathbf{x})\cdot\mathbf{f}_1(\mathbf{x}))(\nabla h(\mathbf{x})\cdot\mathbf{f}_2(\mathbf{x}))>0$ for all $\mathbf{x}\in\Sigma$; an overview can be found in [48]. Some kind of Neĭmark-Sacker bifurcation occurs when a complex pair of Floquet multipliers of a periodic orbit jump from inside to outside the complex unit circle. By varying two parameters, Arnol′d tongues emanate from the corresponding bifurcation curve, though their boundaries are border-collision bifurcations, rather than saddle-node bifurcations. The dynamics near this analog of the Neĭmark-Sacker bifurcation exhibits similar features as for smooth systems, but often the situation is much more complicated. A (discrete-time) piecewise-linear normal form of this scenario is presented in [30] and the resulting phase-locked solutions have been studied in [36, 37, 46, 47]. Using brute-force computational methods, these works present two-parameter diagrams with Arnol′d tongues containing the phase-locked solutions, along with regions that exhibit more complicated dynamics, including chaos. As in [45], the tongues contain shrinking points and the attracting periodic orbit from one sausage to the next in the string differs by having one point move through the switching surface. Hence, the tongues do not actually cross at a shrinking point. Rather, one should interpret a shrinking point as a point where four different border-collision curves meet [37].

In contrast to the research discussed above, we consider Filippov systems of the form (1.1) that do exhibit sliding on the switching surface. The presence of sliding makes the analysis rather different, because trajectories that contain a sliding segment cannot be followed backward in time. Attracting sliding segments have stabilizing effects on the system dynamics. In particular, if a periodic orbit of a two-dimensional system becomes tangent to an attracting sliding region, that is, it undergoes a grazing-sliding bifurcation, then the emanating branch of periodic orbits that contain a sliding segment is always stable even if the periodic orbit was unstable before the tangency [25]. We focus on the grazing-sliding bifurcation as a possible candidate for the Neĭmark-Sacker bifurcation in piecewise-smooth systems. Our motivation comes from the model of a piecewise-smooth friction oscillator that exhibits precisely this type of bifurcation [16]. The grazing-sliding bifurcation is defined as a tangency of a periodic orbit with an attracting sliding region and we assume that the periodic orbit before the grazing-sliding bifurcation is an unstable focus. We already studied this example and derived a normal-form map in [39]. We found that a polygon-shaped attractor coexists with the focus-type unstable periodic orbit before the grazing-sliding bifurcation. In [39] we explained how the number of sides of this

polygon-shaped attractor depends on the system parameters and already observed that the dynamics on the attractor can be chaotic. In this paper we describe the Arnol′d tongues that organize the phase-locked dynamics on the attractor. As was pointed out in [39], the attractor is not necessarily a topological polygon, because the dynamics on its sides may take place on the opposite sides of the vertices. We find that this can also be the case when the dynamics is phase locked, so that the situation cannot be reduced to the dynamics on a circle map. Fortunately, we are able to reduce the system to a one-dimensional induced map based on the construction of Hofbauer towers [20, 22]. The phase-locked solutions can then be found in a way that is similar to the approach in [36], but the use of the induced map avoids the need for checking admissibility of these solutions.

This paper is organized as follows. In the next section we recall the basic features of the piecewise-smooth friction oscillator that was introduced in [39]. We explain the model and derive the normal form used in this paper. We also recall the properties of the polygon-shaped set that contains the attractor which exists before the grazing-sliding bifurcation. Section 3 introduces the one-dimensional induced map and explains how we determine the boundaries of the Arnol′d tongues. Here, we also relate the closing of an Arnol′d tongue to a double border-collision bifurcation and show that such a double border collision happens each time when an Arnol′d tongue crosses a curve where the number of sides of the polygon-shaped invariant set changes. We also prove that at a double border-collision bifurcation a certain iterate of the one-dimensional induced map is equal to the identity. In Sec. 4 we consider stiff smooth systems that are obtained by smoothing either the vector field or the normal form map. As expected from the literature, the shrinking points of piecewise-smooth systems are degeneracies that do not carry over to their smoothed counterparts. The boundaries of the Arnol′d tongues unfold in a manner as predicted by the theory [2]. We end with conclusions in Sec. 5.

2. The piecewise-smooth friction oscillator. We briefly recall the motivating example of a one degree-of-freedom friction oscillator. A schematic of the oscillator is shown in Fig. 1. The oscillator consists of a block mass m that is riding on a constantly moving belt. The displacement of the block mass is denoted by x. The block mass is attached to a damper c that is anchored at the other end, and to a spring s that is harmonically forced with amplitude u_0 and angular frequency ω. We assume a linearly changing friction force with slope κ, that is $F_{\text{friction}} = F_s \operatorname{sgn}(\dot{x}-v_0) - \kappa\,(\dot{x}-v_0)$, where v_0 is the speed of the belt, and F_s is the static friction force. We rescale time, so that the velocity changes to $\dot{x} \mapsto \dot{x}/\sqrt{sm}$, and replace the parameters $F_s \mapsto F_s/s$, $v_0 \mapsto v_0/\sqrt{sm}$, and $\omega \mapsto \omega\sqrt{m/s}$. Then we obtain the equation of motion

$$\dot{\mathbf{x}} = \begin{pmatrix} 0 & 1 \\ -1 & -2\zeta+\kappa \end{pmatrix} \mathbf{x} + \begin{pmatrix} 0 \\ -F_s \operatorname{sgn}(\dot{x}-v_0) - \kappa\, v_0 + u_0 \cos\omega t \end{pmatrix}, \tag{2.1}$$

where $\mathbf{x} = (x, \dot{x})^T$ and $\zeta = c/(2\sqrt{sm})$ is the relative damping.

The animation associated with Fig. 1 shows an example of stick-slip motion [9, 16, 18, 33, 29]. Here, $\zeta = 0.005$, $v_0 = 1$, $\kappa = 1.1152$, $F_s = 1$, $u_0 = 1.078$, and $\omega = 1.6650$. While the relative velocity $\dot{x} - v_0$ between the block mass and the belt is nonzero the block mass is slipping on the belt, which generates a reactive friction force. Note that the mass can slip such that the block moves to the left or right, depending on the sign of $\dot{x}$, but the friction force in this case always points to the right. As soon as $\dot{x} - v_0$ becomes zero, the block sticks to the belt until the inertia of the mass together with the forces of the damper and the spring overcome F_s. Note

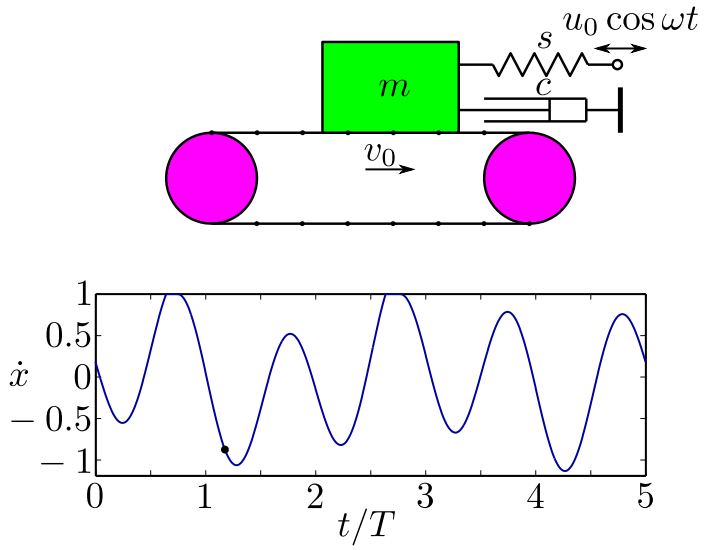

FIG. 1. *Example of stick-slip motion for a piecewise-smooth friction oscillator. The block mass m forms a one-degree-of-freedom oscillator with the spring s and damper c. The block rides on a belt moving with constant speed v_0, and is forced through the spring s with amplitude u_0 and angular frequency $\omega = 2\pi/T$. The velocity profile shows an attracting $5T$-periodic solution with two stick-phases that exists for $\zeta = 0.005$, $v_0 = 1$, $\kappa = 1.1152$, $F_s = 1$, $u_0 = 1.078$, and $\omega = 1.6650$. The accompanying animation* `stickslip-stable.gif` *shows what this solution means in terms of the friction oscillator.*

that, in the terminology of Filippov systems, the *stick-phase* of the motion takes place on the switching surface and corresponds to the dynamics of the *sliding* vector field; while this may be confusing, we will use the Filippov terminology, unless we are in the specific context of the piecewise-smooth friction oscillator.

The piecewise-smooth friction oscillator (2.1) undergoes a grazing-sliding bifurcation at a critical value $\overline{u}_0$ of the forcing amplitude. For $u_0 < \overline{u}_0$ system (2.1) has a unique periodic orbit with $\dot{x} - v_0 < 0$ at all times, that is, the mass is sliding on the belt in an oscillating manner and never sticks. We assume that this periodic orbit is unstable with complex Floquet multipliers, which means that $0 < \kappa - 2\zeta < 2$. If $u_0 = \overline{u}_0$ then there is a single point on the periodic orbit with $\dot{x}(t) = v_0$ and we say that the periodic orbit is grazing the switching surface $\Sigma := \{(x, \dot{x}, t) \in \mathbb{R}^3 \,:\, \dot{x} = v_0\}$. For $u_0 > \overline{u}_0$ the periodic orbit persists as a stable periodic orbit with stick-slip motion. We showed in [39] that, for $u_0 < \overline{u}_0$, an attractor exists on a tubular polygon-shaped invariant set that scales linearly with $\overline{u}_0 - u_0$ and surrounds the (by assumption unstable) periodic orbit. We briefly review this in the next section.

2.1. The Poincaré return map with a discontinuity correction. In order to analyze the dynamics in a neighborhood of the grazing-sliding bifurcation we use a carefully chosen Poincaré return map defined on a section transverse both to the periodic orbit and the switching surface Σ. The Poincaré map models the local dynamics near grazing and incorporates the effects of discontinuity due to sliding. The technique for deriving a Poincaré map was introduced by Nordmark [28] and later refined for grazing-sliding by di Bernardo et al. [12].

We begin by choosing a Poincaré section Π that is perpendicular to the periodic orbit as well as the switching surface Σ at the moment of the grazing-sliding bifurca-

tion, that is, for $u_0 = \overline{u}_0$. This means that any (unstable) periodic orbit with $u_0 < \overline{u}_0$ is transverse to Π as long as u_0 is close enough to $\overline{u}_0$. We now choose a u_0-dependent coordinate system $\mathbf{y} = (y_1, y_2)^T \in \Pi$ that places the intersection of the periodic orbit with Π for each u_0 at the origin. Furthermore, $\mathcal{K}_0 := \Sigma \cap \Pi = \{\mathbf{y} \in \Pi : y_2 = 1\}$ defines the switching line on Π. In these u_0-dependent coordinates the distance between the periodic orbit and Σ, which is small for system (2.1), is scaled to 1. Therefore, the Poincaré map is valid only for $u_0 < \overline{u}_0$ close enough to $\overline{u}_0$ and it does not describe the grazing-sliding bifurcation itself.

The Poincaré return map models the local dynamics that is induced by the grazing-sliding bifurcation and it is well defined also for orbits close to the periodic orbit that do interact with Σ. Indeed, Nordmark [28] expresses the presence of the switching surface in terms of a discontinuity map that is applied only when orbits interact with Σ. For points $\mathbf{y}$ with $y_2 \leq 1$ the Poincaré map is defined as the standard return map of a smooth vector field. As shown in [39], this map is essentially an expanding rotation defined by the matrix

$$M = e^{\beta} \begin{pmatrix} \cos\alpha & \sin\alpha \\ -\sin\alpha & \cos\alpha \end{pmatrix},$$

where we assume $\beta > 0$. If $y_2 > 1$, however, the point corresponds to an orbit of (2.1) with a stick-phase. The discontinuity map amounts to a correction step that projects the point along a particular fixed angle to the switching line $\mathcal{K}_0$. Indeed, the stick-phase of the block mass always ends at a point in phase space with velocity v_0 and the projection angle is determined by the duration of the stick-phase, which to first approximation depends linearly on the distance from the switching line. After the projection, the rotation matrix M can be applied as normal. For our purposes it is more natural to swap the order of projection and rotation. As before, we apply the rotation matrix M to a point with $y_2 \leq 1$, but now we check whether this should be followed by a projection or not. The resulting normal form map then becomes

$$\mathbf{y} \mapsto \begin{cases} M\mathbf{y}, & \text{if} \quad e^{\beta}(y_2\cos\alpha - y_1\sin\alpha) \leq 1, \\ \hat{\mathbf{y}} + JM\mathbf{y}, & \text{if} \quad e^{\beta}(y_2\cos\alpha - y_1\sin\alpha) \geq 1, \end{cases} \tag{2.2}$$

where

$$J = \begin{pmatrix} 1 & \gamma \\ 0 & 0 \end{pmatrix}, \quad \text{and} \quad \hat{\mathbf{y}} = \begin{pmatrix} -\gamma \\ 1 \end{pmatrix}.$$

While this normal form is different from the one defined in [39], it produces entirely equivalent dynamics that now takes place on or below $\mathcal{K}_0$.

The normal form (2.2) is a good approximation of the Poincaré map for the piecewise-smooth friction oscillator (2.1) in a neighborhood of the grazing-sliding bifurcation. The values of the parameters are found as follows:

$$\alpha = \frac{2\pi\sqrt{1-\zeta_r^2}}{\omega}, \quad \beta = -\frac{\zeta_r\alpha}{\sqrt{1-\zeta_r^2}} \quad \text{and} \quad \gamma = \frac{\beta}{\alpha}, \tag{2.3}$$

with $\zeta_r = \zeta - \kappa/2$. Figure 2 compares the normal form (2.2) and the Poincaré map on Π that is obtained from direct integration of the vector field (2.1). Panel (a) shows the dynamics of the Poincaré map using $\zeta = 0.01$, $\kappa = 0.03$, $F_s = 1.0$, $v_0 = 0.103$, $u_0 = 0.2115$, and $\omega = 2.5125$. Iterates quickly converge to a five-sided polygon-shaped chaotic attractor. Since we are close to the grazing-sliding bifurcation, all lines appear

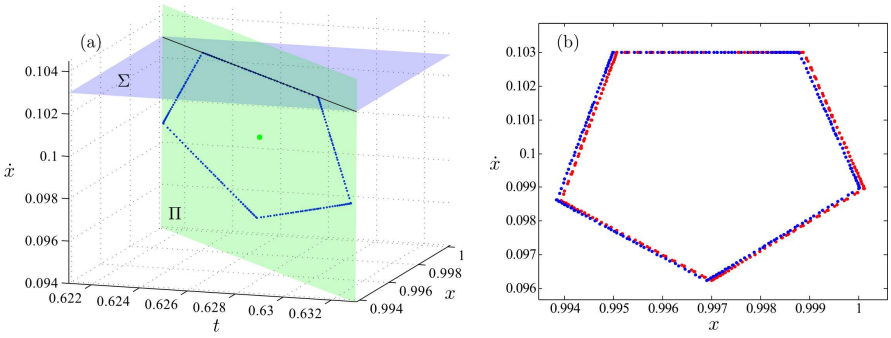

FIG. 2. *An attractor (blue dots) for the Poincaré return map of the piecewise-smooth friction oscillator* (2.1) *with* $\zeta = 0.01$, $\kappa = 0.03$, $F_s = 1.0$, $v_0 = 0.103$, $u_0 = 0.2115$, *and* $\omega = 2.5125$ *is entirely located in the region below and including the switching surface* Σ, *where the relative velocity* $\dot{x} - v_0$ *changes sign (a). Panel (b) shows superimposed the dynamics of the corresponding normal form* (2.2) *(red dots) in the original coordinates on the section* Π *in projection onto the* $(x, \dot{x})$*-plane.*

straight. However, the end of the sliding region in Σ is defined by $\{\dot{x} = v_0, \ddot{x} = 0\}$, which gives $x = F_s - 2\zeta v_0 + u_0 \cos \omega t$ on Σ, where we use $\mathrm{sgn}(\dot{x} - v_0) = -1$; this defines the intersection curve $\mathcal{K}_0 = \Sigma \cap \Pi$. The other sides of the polygon are forward iterates of K_0. Figure 2(b) shows the polygon-shaped attractor in Π projected onto the $(x, \dot{x})$-plane (blue dots). Superimposed is the attractor for the normal form (2.2) using $\alpha = 0.398 \times 2\pi$, $\beta = 0.002$, and $\gamma = 0.005$ (red dots); the iterates of the normal form are transformed back into the original coordinates on Π for comparison. While the normal form (2.2) distorts location of the iterates a little bit, the actual dynamics and shape of the attractor are identical.

2.2. The polygon-shaped attractor. We showed in [39] that the dynamics of the normal form (2.2) essentially takes place on a polygon-shaped attracting invariant set that is obtained by iterating $\mathcal{K}_0$. Indeed, the normal form (2.2) has an unstable fixed point, that is, $\beta > 0$, so that every initial point with $y_2 < 1$ will, after finitely many iterations, be mapped to a point with $y_2 > 1$. This implies that the final rotation step will be followed by a projection and the image will lie on $\mathcal{K}_0 = \Sigma \cap \Pi = \{\mathbf{y} \in \mathbb{R}^2 \,:\, y_2 = 1\}$. Hence, after finitely many steps all the dynamics will be restricted to $\mathcal{K}_0$ and its forward iterates $\mathcal{K}_i := M^i \mathcal{K}_0$. We definine the mininal polygon $\mathcal{P}_f$ as the smallest polygon that is formed by the collection $\{\mathcal{K}_i\}_{i \geq 0}$. The minimal polygon has q sides, for some $3 \leq q < \infty$, and $\mathcal{K}_q$ or any higher iterate of $\mathcal{K}_0$ does not intersect $\mathcal{P}_f$. To distinguish different types of polygons we associate a rational number p/q to every polygon, such that q is the number of sides and p reflects the order of the sides. If $\beta = 0$, then $\mathcal{P}_f$ for $\alpha = 2\pi \frac{p}{q}$ is symmetric and the sides are mapped onto each other with rotation number p/q. For $\beta > 0$ every polygon is a deformed version of a symmetric minimal polygon, so that it inherits the rotation number of the symmetric polygon with the same number and order of sides.

The number of sides of $\mathcal{P}_f$ depends only on the parameters α and β, because the location of $\mathcal{K}_i$ does not depend on the projection direction parameterized by γ. As was explained in [39], the number of sides of $\mathcal{P}_f$ changes when three lines $\mathcal{K}_{n_1}, \mathcal{K}_{n_2}$ and $\mathcal{K}_{n_3}$ intersect at the same point and this point is on the minimal polygon. For a q-sided polygon with p/q side ordering the side removal is organized by the curves in

parameter space defined by

$$e^{q_2\beta}\sin(q_1-q_2)\alpha + e^{(q_2-q_1)\beta}\sin q_2\alpha - \sin q_1\alpha = 0. \tag{2.4}$$

Here, q_1 and q_2 are such that p/q is the Farey sum of the two neighboring rationals $\frac{p_1}{q_1}$ and $\frac{p_2}{q_2}$ on the Farey-tree, that is,

$$\frac{p}{q} = \frac{p_1+p_2}{q_1+q_2}; \tag{2.5}$$

see [15, 19] for more details. The side-removal curves are shown in red in Fig. 4; see also [39].

The purpose of this paper is to investigate the phase-locked dynamics on the polygon-shaped attractor as a function of the parameters α, β and γ. As we already found in [39], we cannot assume that the attractor is topologically a closed curve, because the dynamics takes place on either side of the vertices of $\mathcal{P}_f$.

3. Arnol′d tongues of the piecewise-smooth system. In order to find phase-locked orbits on the attractor, we consider a one-dimensional map that describes how points on $\mathcal{K}_0$ map back to $\mathcal{K}_0$; see also [39]. This map will be an induced map constructed using the Hofbauer towers [20, 22]. We subdivide the line $\mathcal{K}_0$ into intervals from which different numbers of iterations with M are necessary to come back to $\mathcal{K}_0$. For each interval there is a return map f_m that is composed of m expanding rotation steps followed by one projection step. This map is linear and given by

$$u \mapsto f_m(u) := a(m)\,u + b(m),$$

where $a(m) = e^{m\beta}(\cos m\alpha - \gamma\sin m\alpha)$, $b(m) = -\gamma + e^{m\beta}(\sin m\alpha + \gamma\cos m\alpha)$ and $u = y_1$ parameterizes $\mathcal{K}_0$. Any phase-locked orbit will be the fixed point of a finite composition

$$f_{\mathbf{m}}(u) := f_{m_N}\circ\cdots\circ f_{m_2}\circ f_{m_1},$$

for a sequence of iterations $\mathbf{m} = (m_1, m_2, \ldots m_N)$. Indeed, the function

$$u \mapsto f_{\mathbf{m}}(u) := \left[\prod_{i=1}^{N} a(m_i)\right] u + \left[\sum_{i=1}^{N-1} b(m_i)\right]\left[\prod_{j=i+1}^{N} a(m_j)\right] + b(m_N). \tag{3.1}$$

generically has the unique fixed point

$$u^\star_{\mathbf{m}} = \frac{\left[\sum_{i=1}^{N-1} b(m_i)\right]\left[\prod_{j=i+1}^{N} a(m_j)\right] + b(m_N)}{1-\left[\prod_{i=1}^{N} a(m_i)\right]}.$$

Obviously, any cyclic permutation of $\mathbf{m}$ describes the same periodic orbit, but starting with a different point on $\mathcal{K}_0$. Note that the number N of elements in $\mathbf{m}$ determines how many points there are on $\mathcal{K}_0$, that is, how many sliding segments (stick-phases) the solution contains.

Let us first concentrate on periodic orbits that originate from the family at $\beta = 0$ and illustrate this with an example for $q = 5$. Consider the trivial composition with $N = 1$, so that $\mathbf{m} = (q)$. Solving $u = f_{(q)}(u)$, we find the unique fixed point

$$u^\star_{(q)} = \frac{b(q)}{1-a(q)} = \frac{e^{q\beta}(\sin q\alpha + \gamma\cos q\alpha) - \gamma}{1 - e^{q\beta}(\cos q\alpha - \gamma\sin q\alpha)}.$$

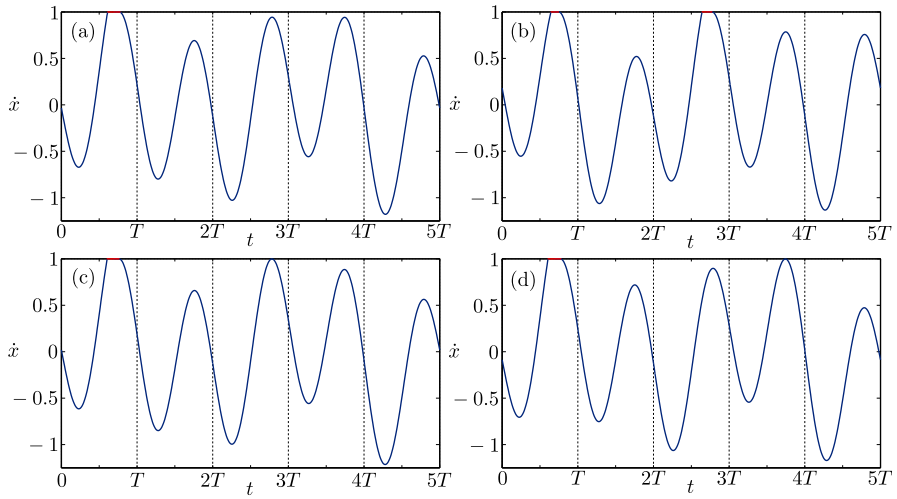

FIG. 3. *Velocity profiles for the vector field* (2.1) *illustrating periodic solutions of the normal form* (2.2) *inside and on the boundaries of the* 2/5 *Arnol′d tongue. The parameters used in* (2.1) *are the same as in Fig. 1 for panels (a) and (b), which corresponds to* $\alpha = 0.404 \times 2\pi$ *and* $\beta = 0.268$, *and* ζ *and* ω *are chosen such that* $\alpha = 0.397 \times 2\pi$ *and* $\beta = 0.263$ *in panel (c), and* $\alpha = 0.411 \times 2\pi$ *and* $\beta = 0.273$ *in panel (d). Panels (a) and (b) show a pair of coexisting saddle and stable periodic orbits inside the* 2/5 *Arnol′d tongue, respectively. These solutions correspond to* $u^\star_{(q)} = u^\star_{(5)}$ *and* $u^\star_{(q_1,q_2)} = u^\star_{(2,3)}$ *that merge in a (left) border collision in panel (c). Panel (d) illustrates the (right) border collision, where* $u^\star_{(q)} = u^\star_{(5)}$ *merges with the equivalent periodic orbit* $u^\star_{(q_2,q_1)} = u^\star_{(3,2)}$. *The accompanying animation* `stickslip-unstable.gif` *shows what the solution in panel (a) means in terms of the piecewise-smooth friction oscillator; see also the animation* `stickslip-stable.gif` *accompanying Fig. 1 that corresponds to panel (b).*

Note that $f'_{(q)}(u^\star_{(q)}) = a(q) = e^{q\beta}(\cos q\alpha - \gamma \sin q\alpha)$, so that $u^\star_{(q)}$ is unstable (of saddle type) for α close to $2\pi\frac{p}{q}$ and $\beta > 0$. The velocity profile for a solution of the piecewise-smooth friction oscillator (2.1) that corresponds to $u^\star_{(q)}$ with $q = 5$ is shown in Fig. 3(a). Here, we used the same parameters as in Fig. 1, which is equivalent to using $\alpha \approx 0.404 \times 2\pi$, $\beta \approx 0.268$, and $\gamma = \beta/\alpha$. For this choice of parameters the minimal polygon $\mathcal{P}_f$ has $q = 5$ sides and $p/q = 2/5$ side ordering. Hence, the solution in Fig. 3(a) corresponds to a periodic orbit of (2.2) with rotation number 2/5. Note that the velocity profile has been shifted in time so that the stick-phase is happening in the middle of the first return $[0, T]$, where T is the forcing period $2\pi/\omega$. The stick-phase, or sliding segment where $\dot{x} = 1$ (marked in red), takes place only during the $[0, T]$ interval, and $\dot{x} < 1$ for the next four returns. The animation associated with Fig. 3(a) illustrates the motion of the mass on the belt that corresponds to this solution.

The (saddle) periodic orbit $u^\star_{(q)} = u^\star_{(5)}$ coexists with the stable periodic orbit of Fig. 1, which is reproduced in Fig. 3(b). This stable periodic orbit is the unique fixed point $u^\star_{(q_1,q_2)} = u^\star_{(2,3)}$ with $\mathbf{m} = (q_1, q_2)$ formed by the denominators of the Farey neighbors $\frac{p_1}{q_1} = \frac{1}{2} > \frac{p_2}{q_2} = \frac{1}{3}$ of $\frac{p}{q}$, i.e., $q_1 + q_2 = q$. The stability of $u^\star_{(q_1,q_2)}$ is determined by $f'_{(q_1,q_2)}(u^\star_{(q_1,q_2)}) = a(q_1)a(q_2)$. Using $q_2 = q - q_1$, we have

$$\begin{aligned} a(q_1)a(q_2) &= e^{q_1\beta}(\cos q_1\alpha - \gamma \sin q_1\alpha)\; e^{(q-q_1)\beta}(\cos{(q-q_1)}\alpha - \gamma \sin{(q-q_1)}\alpha) \\ &= e^{q\beta}\left([1 - (1+\gamma^2)\sin^2 q_1\alpha]\,\cos q\alpha + [-\gamma + \tfrac{1}{2}(1+\gamma^2)\sin 2q_1\alpha]\,\sin q\alpha\right). \end{aligned}$$

Let us first consider $\alpha = 2\pi\frac{p}{q}$, that is, $\cos q\alpha = 1$ and $\sin q\alpha = 0$. Note that $q_1\alpha = 2\pi(p_1 - \frac{1}{q})$, because any Farey sequence $\frac{p_2}{q_2} < \frac{p}{q} < \frac{p_1}{q_1}$ satisfies $q_1p - p_1q = -1$ and $q_2p - p_2q = 1$; see [15, 19]. Hence, the equation becomes

$$a(q_1)a(q_2)|_{\alpha=2\pi\frac{p}{q}} = e^{q\beta}\left(1 - (1+\gamma^2)\sin^2\left[\tfrac{2\pi}{q}\right]\right),$$

so that $u^\star_{(q_1,q_2)}$ is stable for $\alpha = 2\pi\frac{p}{q}$ and β sufficiently small, provided $-1 < \gamma < 1$, which is the case for the piecewise-smooth friction oscillator (2.1). Clearly, stability is then also preserved for α close to $2\pi\frac{p}{q}$.

The two periodic orbits $u^\star_{(q)} = u^\star_{(5)}$ and $u^\star_{(q_1,q_2)} = u^\star_{(2,3)}$ form a pair of phase-locked periodic orbits on $\mathcal{P}_f$. Since their rotation numbers are $2/5$, the orbits correspond to a point inside the $2/5$ Arnol′d tongue. Using a brute-force method, we could now scan the entire (α,β)-parameter space for a fixed choice of γ and find how the Arnol′d tongues organize parameter space. This is the method used in [36, 47, 48]. However, in the spirit of dynamical systems theory, it is much more efficient to compute the boundaries of these tongues. If we follow the periodic orbits in Figs. 3(a) and (b) in the direction of decreasing α, we find that they merge into the solution shown in Fig. 3(c); here $\alpha = 0.397 \times 2\pi$ and $\beta = 0.263$, that is, we used the values as in Fig. 1, but adjusted ζ and ω to match the new values of α and β; note that again $\gamma = \beta/\alpha$. Figure 3(c) shows how the second sliding segment of $u^\star_{(q_1,q_2)} = u^\star_{(2,3)}$ in the third forcing period has contracted to a single point; similarly, the periodic orbit $u^\star_{(q)} = u^\star_{(5)}$ of Fig. 3(a) has developed a tangency with $\mathcal{K}_0$ in the third forcing period. In terms of the normal form (2.2) this means that α, β and γ are such that the q_1th = 2nd of the q iterations with M starting with headpoint $u^\star_{(q)} = u^\star_{(5)}$ on the line $\mathcal{K}_0 = \{(y_1,y_2)^T \in \mathbb{R}^2 : y_2 = 1\}$ falls exactly on $\mathcal{K}_0$. Similarly, if we follow the periodic orbits in Figs. 3(a) and (b) in the direction of increasing α, they merge into the solution shown in Fig. 3(d), where $\alpha = 0.411 \times 2\pi$ and $\beta = 0.273$. Note that $u^\star_{(q)} = u^\star_{(5)}$ has now developed a tangency with $\mathcal{K}_0$ in the fourth forcing period, that is, the q_2th = 3rd iteration with M falls exactly on $\mathcal{K}_0$.

The merging and subsequent disappearance of a pair of stable and saddle periodic orbits as described above in a piecewise-linear system is called a border-collision bifurcation of creation-annihilation type [11]. The border-collision bifurcations form the boundaries of the Arnol′d tongues for $\beta > 0$ small enough. As also happens for smooth systems [5, 32], additional bifurcations may happen inside the Arnol′d tongues for larger β. However, similar to what was reported in [37, 47, 48], the boundaries of the Arnol′d tongues are characterized by border-collision bifurcations of phase-locked pairs of periodic orbits. We make this more precise in the next section.

3.1. Border collisions as boundaries of Arnol′d tongues. A periodic orbit undergoes a border-collision bifurcation if one of the iterates with M of the headpoint $u^\star_{\mathbf{m}}$ falls on the line $\mathcal{K}_0 = \{(y_1,y_2)^T \in \mathbb{R}^2 : y_2 = 1\}$. This condition is stipulated by the equation

$$\mathsf{BC}(u^\star_{\mathbf{m}}, k) = e^{k\beta}(\cos k\alpha - u^\star_{\mathbf{m}}\sin k\alpha) - 1 = 0. \tag{3.2}$$

Note that this condition can only be applied as long as $0 < k \le m_1$. Therefore, for higher iterates a different headpoint must be selected using a cyclic permutation of $\mathbf{m}$ and this way all the points of the orbit can be checked.

Recall the coexisting pair of periodic orbits $u^\star_{(q)}$ and $u^\star_{(q_1,q_2)}$ on $\mathcal{P}_f$ with q sides and p/q side ordering; let us assume that $q_1 < q_2$. The pair exists for α close to $2\pi\frac{p}{q}$

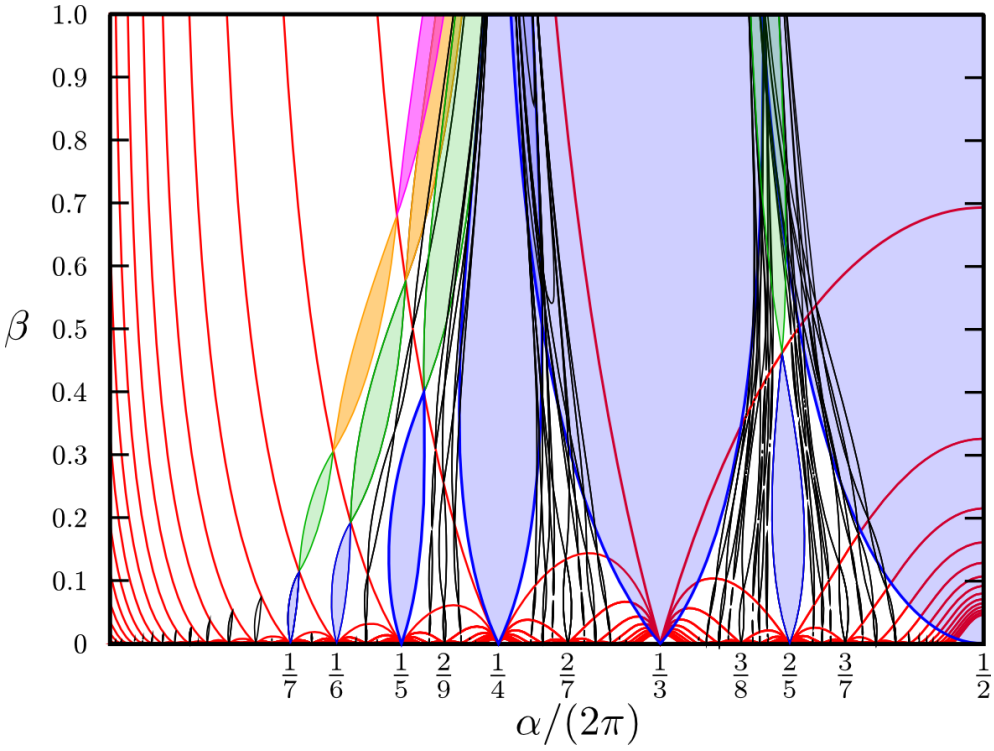

FIG. 4. *Arnol′d tongues in the (α, β)-plan for the normal form (2.2) with $\gamma = 0$. The Arnol′d tongues originate from the line $\beta = 0$ and close up each time when they cross the side-removal curves as defined in (2.4) (shown in red). The first levels (sausages) of the strongest resonance tongues are shaded blue, the second green, the third orange and the fourth magenta.*

and $\beta > 0$ small. (We lose uniqueness for $\beta = 0$, because then $f_{\mathbf{m}}$ is the identity.) We claimed that q_1 and q_2 must be the denominators of the Farey neighbors of $\frac{p}{q}$. Indeed, at the boundary of its existence $u^\star_{(q)}$ undergoes a border-collision bifurcation with another orbit that has one more point on $\mathcal{K}_0$. Hence, at the border-collision bifurcation, $u^\star_{(q)}$ must get an additional point on $\mathcal{K}_0$ from a neighboring side of $\mathcal{P}_f$. Using (2.4), we know that the sides of $\mathcal{P}_f$ adjacent to $\mathcal{K}_0$ are $\mathcal{K}_{q_1}$ and $\mathcal{K}_{q_2}$, where q_1 and q_2 are as above. Therefore, the border-collision bifurcations are defined by

$$\mathsf{BC}(u^\star_{(q)}, q_1) = 0 \quad \text{and} \quad \mathsf{BC}(u^\star_{(q)}, q_2) = 0, \tag{3.3}$$

that is, $\mathbf{m} = (q)$ and $k = q_1, q_2$ in (3.2). This automatically means that the defining map of the other periodic orbit is $f_{(q_1,q_2)}$ or, equivalently, $f_{(q_2,q_1)}$. At the border-collision bifurcation with $\mathsf{BC}(u^\star_{(q)}, q_1) = 0$, the unique fixed point $u^\star_{(q_1,q_2)}$ of $f_{(q_1,q_2)}$ is identical to the unique fixed point $u^\star_{(q)}$ of $f_{(q)}$, because one of their points lies on $\mathcal{K}_0 \cap \mathcal{K}_{q_1}$. For the border-collision bifurcation with $bc(u^\star_{(q)}, q_2) = 0$, we must switch to the other headpoint of $u^\star_{(q_1,q_2)}$ and use the point $u^\star_{(q_2,q_1)}$ that is determined as the unique fixed point of $f_{(q_2,q_1)}$ instead. At the moment of this border-collision bifurcation $u^\star_{(q)}$ has an additional point on $\mathcal{K}_0$ that lies on the intersection with $\mathcal{K}_{q_2}$.

Using the above procedure, we can systematically find the boundaries of Arnol′d tongues, say, up to any given level in the Farey tree. Figure 4 gives an impression of how the tongues are organized in the (α, β)-plane for $\gamma = 0$. We find that all

tongues appear to have tips at $\beta = 0$ generated by transverse intersections of pairs of border-collision curves (3.3). With the exception of the strong resonances 1/2, 1/3 and 1/4, each pair of border-collision curves has another transverse intersection for some value of $\beta \neq 0$; the first six sausage-shaped regions enclosed by the curves (3.3) are shaded blue in Fig. 4. We call the points where the Arnol′d tongues close double border-collision points. Note that this first set of (blue) sausages closes up precisely when a sausage meets the (red) side-removal curves (2.4); we discuss this in detail in Sec. 3.2.

Beyond a double border-collision point, any periodic orbit with headpoint $u^\star_{(q_1,q_2)}$ continues to exist, but is now of saddle type. Since we also crossed a side-removal curve, $u^\star_{(q_1,q_2)}$ resides on a q_2-sided polygon with side ordering p_2/q_2 (we assume $q_2 > q_1$); its rotation number is still p/q. The coexisting stable periodic orbit can be found in the same way as before: $u^\star_{(q_1,q_2)}$ undergoes a (creation-annihilation) border-collision bifurcation and an additional point of the orbit moves onto $\mathcal{K}_0$. The two border-colliding points are uniquely defined as the points closest to $\mathcal{K}_0$ on the neighboring sides of $\mathcal{P}_f$, which are determined by the Farey neighbors $\frac{p_3}{q_3}$ and $\frac{p_4}{q_4}$ of $\frac{p_2}{q_2}$, two levels up from $\frac{p}{q}$ in the Farey tree. Obviously, $q_3, q_4 < q_2 = q_3 + q_4$, such that the left and right border-collision bifurcations are defined using $\mathbf{m} = (q_2, q_1)$ and $k = q_3, q_4$ in (3.2), namely

$$\mathsf{BC}(u^\star_{(q_2,q_1)}, q_3) = 0 \quad \text{and} \quad \mathsf{BC}(u^\star_{(q_2,q_1)}, q_4) = 0$$

Hence, $u^\star_{(q_2,q_1)}$ collides with the stable periodic orbit $u^\star_{(q_3,q_4,q_1)}$ in the left border-collision bifurcation (assume $q_3 < q_4$) and with the equivalent periodic orbit $u^\star_{(q_4,q_1,q_3)}$ in the left border-collision bifurcation. The solutions to these implicit equations give the next level of the Arnol′d tongues, which are shaded green in Fig. 4. Again, at this second level the tongues close up, except when $p_2/q_2 \in \{1/2, 1/3, 1/4\}$.

Additional levels of the Arnol′d tongues can be found similarly; the next two levels are shaded orange and magenta, respectively. In general, we assume that we have a periodic orbit $u^\star$ with rotation number $\frac{p}{q}$ and N points on $\mathcal{K}_0$. The q points of the orbit are ordered according to its rotation number, that is, the consecutive points on $\mathcal{P}_f$ are a permutation $\{n_0, \ldots, n_{q-1}\}$ of the successive iterates $i = 0, \ldots q-1$ of the headpoint, which are determined by

$$n_k = i, \quad \text{with} \quad k = i\,p \,(\mathrm{mod}\, q), \quad 0 \leq i < q.$$

Here, $n_0 = 0$ represents the headpoint and the first N points $\{n_0, \ldots, n_{N-1}\}$ lie on $\mathcal{K}_0$. The function $f_{\mathbf{m}}$ that has $u^\star$ as its fixed point is determined as follows. We sort the numbers $\{n_0, \ldots, n_{N-1}\}$ in increasing order to obtain $\{\hat{n}_0 = 0 < \hat{n}_1 < \cdots < \hat{n}_{N-1}\}$. The sequence of iterations $\mathbf{m} = (m_1, m_2, \ldots m_N)$ is determined by the number of iterations needed each time to return to $\mathcal{K}_0$. Hence, $m_1 = \hat{n}_1 - \hat{n}_0$, $m_2 = \hat{n}_2 - \hat{n}_1$, and so on, until $m_N = q - \hat{n}_{N-1}$.

A border-collision bifurcation happens when a point from a neighboring side of P_f lies on $\mathcal{K}_0$. Note that we cannot assume that P_f has q sides. The minimal polygon P_f will have q_k sides and p_k/q_k side ordering, where $\frac{p_k}{q_k}$ is a Farey neighbor of $\frac{p}{q}$ higher up in the Farey tree. Suppose that the Farey neighbors of $\frac{p_k}{q_k}$ on the same level in the Farey tree are $\frac{p_{k-1}}{q_{k-1}}$ and $\frac{p_{k+1}}{q_{k+1}}$, that is, $p_{k-1}+p_{k+1} = p_k$ and $q_{k-1}+q_{k+1} = q_k$. Then the sides adjacent to $\mathcal{K}_0$ are $\mathcal{K}_{q_{k-1}}$ and $\mathcal{K}_{q_{k+1}}$ and they contain the points n_{q-1} and n_N that are the neighbors of n_0 and n_{N-1}, respectively. Hence, there exists an integer l such that $0 < q_{k-1} \leq m_{l+1}$ and the point n_l on $\mathcal{K}_0$, after $q_{k-1} = n_{q-1} - \sum_{i=1}^{l} m_i$ iterations,

maps to $\mathcal{K}_0 \cap \mathcal{K}_{q_{k-1}}$ (we assume $q_{k-1} < q_{k+1}$). The border-collision bifurcation is then defined implicitly as

$$\mathsf{BC}(u^{\star}_{\tilde{\mathbf{m}}}, q_{k-1}) = 0,$$

where $\tilde{\mathbf{m}}$ is the permutation of $\mathbf{m}$ that starts with m_{l+1}. A similar argument holds for n_N and $\mathcal{K}_{q_{k+1}}$ to find the other border-collision bifurcation curve.

3.2. Closing of Arnol′d tongues at double border-collision points. As we already discussed in the introduction, the closing of Arnol′d tongues in piecewise-linear systems has been observed before [36, 45, 47]. In fact, this phenomenon has also been observed in smooth systems in the context of reversible systems. Sausage-shaped regions, referred to as instability pockets, have been reported for a class of Mathieu equations (in particular, in Hill's equations) [2, 3, 4]. The closing of Arnol′d tongues is structurally stable due to the reversibility of these systems, but for general dissipative systems it is degenerate; see Fig. 6 in [3] and Figs. 5 and 7 in [4]. Simpson and Meiss [37] suggest that the closing of the Arnol′d tongues in piecewise-smooth systems is structurally stable only in the piecewise-linear normal form. However, we believe that in systems with sliding the phenomenon is generic. As illustrated in Fig. 2, the dynamics of the normal form (2.2) is extremely similar to that of the friction oscillator (2.1) and the piecewise-smooth polygon-schaped invariant set appears to behave in the same way as the piecewise-linear polygon of the normal form.

The closing of the Arnol′d tongues in piecewise-smooth systems with sliding is mediated by a double border-collision bifurcation. As an example, consider again the 2/5 Arnol′d tongue in Fig. 4. We discussed the border-collision bifurcations for a pair of periodic orbits in the blue shaded sausage by moving towards the boundaries of the tongue in the direction of decreasing and increasing α; see Fig. 3. This scenario is illustrated again in the first row of Fig. 5 for a cross-section with constant $\beta = 0.23$ and $\gamma = 0$; see panels (a)–(c). The stable and saddle periodic orbits are denoted by blue triangles and green crosses, respectively. Figure 5(b) shows a phase portrait that corresponds to a situation similar to Figs. 3(a) and (b). The periodic orbits lie on a five-sided minimal polygon $\mathcal{P}_f$ and the stable orbit has two points on $\mathcal{K}_0$. Note that the dynamics appears to take place on a topological circle. The left border-collision bifurcation is shown in Fig. 5(a) and the right border-collision bifurcation in Fig. 5(c). The accompanying animation `tongue2-5first.gif` shows how the configuration of the two periodic orbits changes as α increases from 2.45566, approximately at the left border-collision bifurcation, to 2.5562, approximately at the right border-collision bifurcation. This reconfiguration is the same as what happens for smooth systems; for example, see [35].

A similar scenario is shown in Figs. 5(d)–(f), where $\beta = 0.4$; we have moved up higher in the Arnol′d tongue, but are still inside the first blue shaded sausage. Note that the intersection points for two sides of $\mathcal{P}_f$ are much closer together and $\mathcal{P}_f$ is about to lose these sides as β is increased further. In the accompanying animation `tongue2-5closeDBC.gif` one observes that the saddle periodic orbit hardly moves at all, but otherwise, the situation is equivalent to that in the first row of Fig. 5. In particular, the dynamics still takes place on a topological circle. Note that the length of the segment of $\mathcal{K}_0$ on which the periodic orbits reside virtually does not change.

The third row of Fig. 5 shows the situation for $\beta = 0.52$, which is inside the second green shaded sausage. The pair of period-5 orbits now resides on a three-sided polygon and the stable orbit has three points on $\mathcal{K}_0$. Interestingly, the points of the stable periodic orbit no longer lie on the topological circle generated by a three-sided

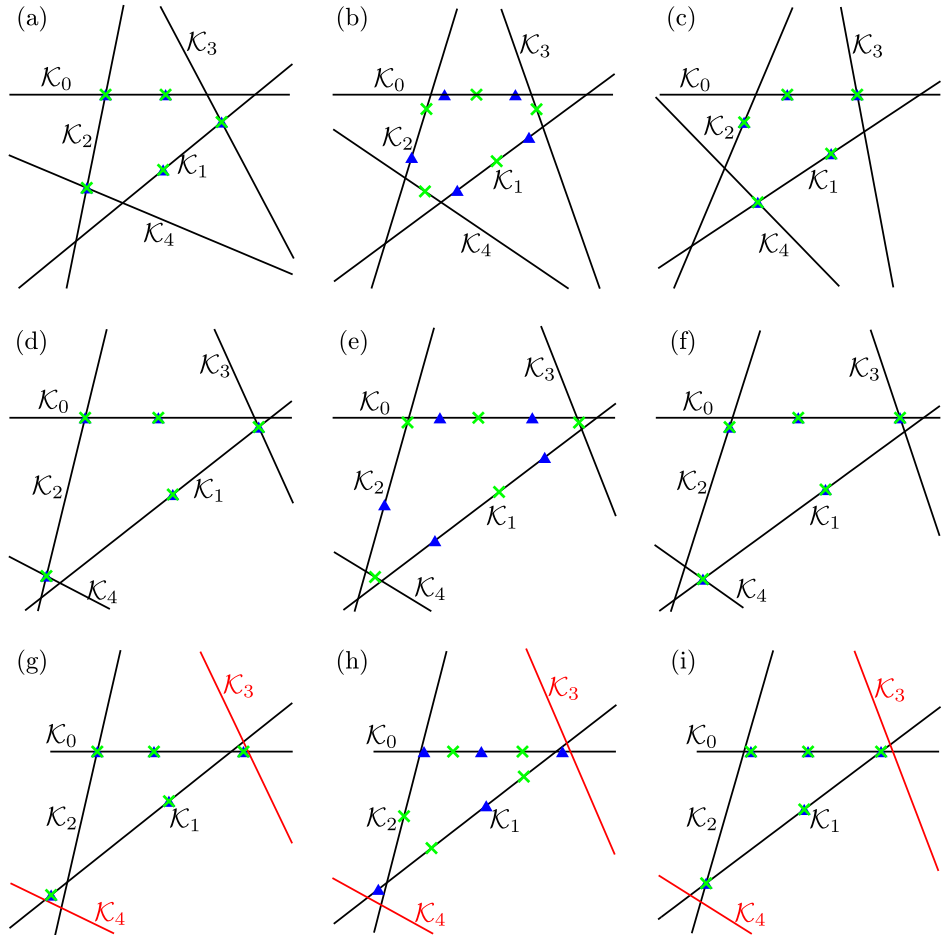

FIG. 5. *Configurations of stable (blue triangles) and saddle (green crosses) periodic points inside and at the boundaries of the* 2/5 *Arnol′d tongue for* $\gamma = 0$. *From top to bottom, each row represents a cross-section for constant* $\beta = 0.23$, $\beta = 0.4$, *and* $\beta = 0.52$, *respectively. The values for* α *are* 2.45566 2.50596, 2.5562, 2.47611, 2.49321, 2.51031, 2.46905, 2.48274, *and* 2.49643 *for panels (a)–(i), respectively. The first and third columns correspond to left and right border-collision bifurcations, respectively, and the middle column shows a phase portrait inside the tongue. The cross-section illustrated in panels (a)–(c) is inside the first sausage; that in panels (d)–(f) is also inside the first sausage, but very close to the double border-collision point; and that in panels (g)–(i) is inside the second sausage. The accompanying animations* `tongue2-5first.gif`, `tongue2-5closeDBC.gif`, *and* `tongue2-5second.gif` *are for the respective cross-sections in rows one to three.*

minimal polygon $\mathcal{P}_f$. As we already reported in [39], this phenomenon may give rise to complex behavior, including chaos, and the stable periodic orbit may well lose stability through other bifurcations as we move higher up inside the tongue. We do not investigate such other bifurcations here. Moreover, note that tongues overlap in Fig. 4, which also gives rise to more complex dynamics and which we do not investigate further.

Figures 4 and 5 suggest that whenever a border-collision curve crosses a side-removal curve, the Arnol′d tongue closes up. In fact, this is always the case and we have the following theorem.

THEOREM 3.1. *Suppose* (2.2) *has a periodic orbit* $u^\star$ *with rotation number* $\frac{p}{q}$ *that*

resides on a q_k-sided minimal polygon $\mathcal{P}_f$ with side ordering p_k/q_k. Assume further that α and β in (2.2) are such that $u^\star$ undergoes a border-collision bifurcation and at the same time $\mathcal{P}_f$ has a triple intersection point. Then $u^\star$ undergoes a double border-collision bifurcation.

Proof. Recall that a triple intersection point of $\mathcal{P}_f$ is defined by the implicit equation (2.4), where the values for q_1 and q_2 must be taken as the denominators of the Farey neighbors of p_k/q_k. Let us denote these by q_l and q_r, with $q_l + q_r = q_k$. As we discussed before, the left and right neighbors of $\mathcal{K}_0$ are then $\mathcal{K}_{q_l}$ and $\mathcal{K}_{q_r}$, respectively. If $u^\star$ undergoes a left border-collision bifurcation then there is a point of $u^\star$ on $\mathcal{K}_0$ that is mapped after q_l iterates onto the intersection point $\mathcal{K}_0 \cap \mathcal{K}_{q_l}$; similarly, if $u^\star$ undergoes a right border-collision bifurcation then there is a point of $u^\star$ on $\mathcal{K}_0$ that is mapped after q_r iterates onto $\mathcal{K}_0 \cap \mathcal{K}_{q_r}$. Note that the headpoints used in these iterations need not be the same. Let us assume that $u^\star$ undergoes a right border-collision bifurcation and the defining equation uses the iteration sequence $\mathbf{m}$ starting with headpoint $u^\star_{\mathbf{m}}$. Hence, using (3.2),

$$\begin{aligned} &\mathsf{BC}(u^\star_{\mathbf{m}}, q_{k+1}) = e^{q_{k+1}\beta}(\cos q_{k+1}\alpha - u^\star_{\mathbf{m}} \sin q_{k+1}\alpha) - 1 = 0 \\ \Leftrightarrow\ & u^\star_{\mathbf{m}} = \frac{e^{q_{k+1}\beta}\cos q_{k+1}\alpha - 1}{e^{q_{k+1}\beta}\sin q_{k+1}\alpha}. \end{aligned}$$

However, we are on a side-removal curve and using (2.4) for q_{k-1} and q_{k+1}, we have

$$\begin{aligned} & e^{q_{k+1}\beta}\sin(q_{k-1} - q_{k+1})\alpha + e^{(q_{k+1}-q_{k-1})\beta}\sin q_{k+1}\alpha - \sin q_{k-1}\alpha = 0 \\ \Leftrightarrow\ & e^{q_{k+1}\beta}\sin q_{k-1}\alpha\cos q_{k+1}\alpha - \sin q_{k-1}\alpha \\ & \quad = e^{q_{k+1}\beta}\sin q_{k+1}\alpha\cos q_{k-1}\alpha - e^{(q_{k+1}-q_{k-1})\beta}\sin q_{k+1}\alpha \\ \Leftrightarrow\ & \frac{e^{q_{k+1}\beta}\cos q_{k+1}\alpha - 1}{e^{q_{k+1}\beta}\sin q_{k+1}\alpha} = \frac{e^{q_{k-1}\beta}\cos q_{k-1}\alpha - 1}{e^{q_{k-1}\beta}\sin q_{k-1}\alpha}. \end{aligned}$$

Hence, $\mathsf{BC}(u^\star_{\mathbf{m}}, q_{k-1}) = 0$ as well, that is, the headpoint for the right border collision is also $u^\star_{\mathbf{m}}$ and the two border-collision bifurcations happen for the same values of α and β. □

As can be seen in Fig. 4, the double border-collision bifurcations generally occur on side-removal curves, although they may occur elsewhere in the parameter space. For example the Arnol′d tongue in between the 1/6 and the 1/5 tongues (this is the 2/11 tongue) has an additional double border-collision bifurcation in the region where the periodic orbits reside on a five-sided minimal polygon. Effectively, this means that there are at least two iterates of a fixed point $u^\star_{\mathbf{m}}$ on a side that will be removed at the next side-removal curve. These points will land on $\mathcal{K}_0$ for different values of α and β and only the last one will fall on the side-removal curve.

If there is a double border-collision bifurcation, then the dynamics on the polygon is a rigid rotation. This is the same phenomenon that occurs in piecewise-linear continuous circle maps [7, 45] and also for reversible systems [2].

THEOREM 3.2. *Suppose (2.2) has a periodic orbit $u^\star$ with rotation number $\frac{p}{q}$ residing on a minimal polygon $\mathcal{P}_f$, and the parameters α and β are such that a double border-collision bifurcation occurs. Then the qth iterate of (2.2) on $\mathcal{P}_f$ is the identity.*

Proof. The periodic orbit $u^\star$ consists of q points that are ordered according to the rotation number $\frac{p}{q}$. At a double border-collision bifurcation there are $N+1$ points of $u^\star$ on $\mathcal{K}_0$, the first and last of which are on the intersections of $\mathcal{K}_0$ with its neighboring sides. As before, we label the points of $u^\star$ by the their iteration numbers $i = 0, \dots q-1$ to obtain the permutation $\{n_0, \dots, n_{q-1}\}$, where $n_0 = 0$ corresponds to the first point

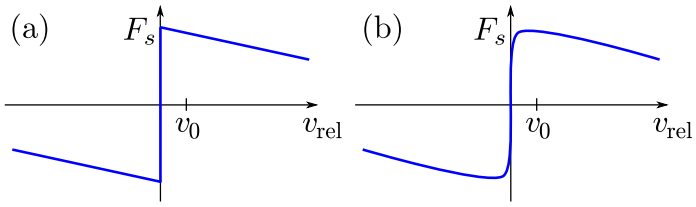

FIG. 6. *The non-smooth (a) and smoothed (b) friction forces as a function of the relative velocity* $v_{\rm rel} = \dot{x} - v_0$.

on $\mathcal{K}_0$ and $\{n_0, \ldots, n_N\}$ with $n_i = n_{i-1} + p$ are all points on $\mathcal{K}_0$. Using only the first N points on $\mathcal{K}_0$, we now construct the sequence of iterations $\mathbf{m} = (m_1, m_2, \ldots m_N)$ that are needed to return to these first N points on $\mathcal{K}_0$. Since we are at a double border-collision bifurcation, one of these first N headpoints maps to the point with label n_N. More precisely, there exists $0 \leq r < N$ such that the point with label n_r on $\mathcal{K}_0$, which maps back to one of the first N points on $\mathcal{K}_0$ after m_r iterates, also maps to n_N already after q_r iterates for some $0 < q_r \leq m_r$. Hence, the periodic orbit $u^\star$ can be viewed as the fixed point $u^\star_{\mathbf{m}}$ with label n_0 of the map $f_{\mathbf{m}}$ defined in (3.1). Now consider the last N points $\{n_1, \ldots, n_N\}$ on $\mathcal{K}_0$. Since the number of points on $\mathcal{K}_0$ is the same and $\{n_1, \ldots, n_N\} = \{n_0 + p, \ldots, n_{N-1} + p\}$, the map (3.1) that generates the fixed point with label n_1 must be the exact same map $f_{\mathbf{m}}$ that generates the fixed point $u^\star_{\mathbf{m}}$ with label n_0. Hence, $f_{\mathbf{m}}$ has two distinct fixed points. Since $f_{\mathbf{m}}$ is linear it must be the identity. Note that the points with labels n_0 and n_1 are always two different points on $\mathcal{K}_0$, because the length of the segment on $\mathcal{K}_0$ on which $u^\star$ resides is always nonzero. □

4. Regularizations of the piece-wise smooth friction oscillator. It is often overlooked in the literature that piecewise-smooth models arise as simplifications of the actual underlying physics. Instead of an actual discontinuity in the vector field, one should probably consider a smooth transition, albeit with a very steep slope. Hence, the regularization of piecewise-smooth systems typically leads to systems with multiple time scales. Particularly in the context of systems with sliding, there have been ideas on how to view the sliding surface as a slow manifold [6, 42, 43].

We consider two different ways of smoothing the discontinuity in the friction force for the friction oscillator (2.1), namely, in the next section we smooth this friction force directly and in Sec. 4.2 we consider a smoothed version of the normal form (2.2) as the approximation of a smoothed Poincaré return map. It may come as no surprise that these two approaches lead to different results, but we find that the smoothing of the normal form also brings out the essence of sliding versus piecewise-smooth dynamics without sliding.

4.1. Smoothed vector field. The only nonsmooth part in the governing equation of the vector field (2.1) is the friction force $F_{\rm friction} = F_s \operatorname{sgn}(\dot{x} - v_0) - \kappa\,(\dot{x} - v_0)$. Figure 6(a) shows the graph of $F_{\rm friction}$ versus the relative velocity $v_{\rm rel} = \dot{x} - v_0$. We replace this function with the smooth function depicted in Fig. 6(b), where the signum function is approximated by an appropriately scaled analytic tanh function; this idea was also used in [25]. The smoothed vector field is then given by

$$\dot{\mathbf{x}} = \begin{pmatrix} 0 & 1 \\ -1 & -2\zeta_r \end{pmatrix} \mathbf{x} + \begin{pmatrix} 0 \\ -F_s \tanh C(\dot{x} - v_0) - \kappa\, v_0 + u_0 \cos \omega t \end{pmatrix}, \qquad (4.1)$$

with $\zeta_r = \zeta - \kappa/2$ as before. Equation (4.1) is now solvable with conventional ordinary differential equation solvers, although the dynamics is rather stiff in the regions where the friction force changes sign. The parameter C is a smoothing parameter that controls this stiffness; it is kept constant at $C = 3000$ in our calculations. The other parameters we use are $\kappa = 0.005$, $F_s = 1$ and $v_0 = 1$, while ω and ζ_r are the bifurcation parameters. Note that sliding is not possible in (4.1). In order to control the distance of the periodic orbit from the switching surface Σ we introduce another parameter ϱ that scales the forcing amplitude from the zero-amplitude periodic orbit at $\varrho = 0$ to the grazing orbit at $\varrho = 1$, that is,

$$u_0 = -\varrho\, v_0 \sqrt{(1-\omega^{-2})^2 + 4\zeta_r^2}.$$

The two parameters C and ϱ have opposite effects in terms of smoothing. If we increase ϱ the interesting dynamics will occur in a smaller neighborhood of Σ. However, the neighborhood of Σ in which the dynamics is smoothed is determined by C. Therefore, the effect of large C diminishes if ϱ is increased, leading to locally smoother dynamics. Hence, the closer ϱ is to 1 the more challenging it becomes to overcome the stiffness of the system.

Our aim is to compare Arnol′d tongues computed for the Poincaré return map of (4.1) with those for the normal form (2.2). The normal form and, in particular, the projection matrix J provide a good approximation if the sliding segments of the grazing-sliding orbits are short, which is the case near grazing. Hence, in order to obtain a good comparison between the smoothed vector field and the normal form, we must set ϱ as close to 1 as possible. We found that $\varrho = 0.95$ was the largest value we could use to reliably compute the periodic orbits, but this restricts the range of $|\zeta_r|$ and, consequently, the range of β.

Since (4.1) is now a smooth vector field, the boundaries of the Arnol′d tongues are saddle-node bifurcations. We used PDDE-CONT [38] to follow these saddle-node bifurcation curves in the two parameters ζ_r and ω and transformed the result back into the (α, β)-plane using (2.3). Figure 7 shows the results of our computation superimposed on the Arnol′d tongues of the normal form computed with varying $\gamma = \beta/\alpha$; note that the use of a non-constant γ does not really alter the structure of the Arnol′d tongues, though the two-parameter diagram is slightly different from that in Fig. 4 where we used $\gamma = 0$. The saddle-node bifurcation curves of (4.1) are black and the corresponding border-collision bifurcation curves of (2.2) are red. The green curves are other border-collision bifurcation curves of (2.2). For small values of β the Arnol′d tongues agree well, but for larger β-values they diverge. This is primarely due to the increasing length of the sliding segments for which the projection matrix J in (2.2) cannot account. We also encountered other bifurcations higher up in the tongues that correspond to non-smooth bifurcations other than grazing-sliding bifurcations.

The enlargments in Figs. 7(b) and (c) show that the Arnol′d tongues do not close in the smoothed vector field. This deformation is very similar to what happens for nonreversible perturbations of Hill's equations; see Fig. 5 in [4].

4.2. Smoothed map. Instead of regularizing the vector field directly, one can also consider smoothing the normal form (2.2). We achieve this by using the same tanh function as in (4.1) to smooth the transition from pure rotation to pure projection:

$$\mathbf{y} \mapsto \frac{(1+\tanh C(1-y_2))}{2}\, M\,\mathbf{y} + \frac{(1+\tanh C(y_2-1))}{2}\,(\hat{\mathbf{y}} + M\, J_\epsilon\, \mathbf{y}), \tag{4.2}$$

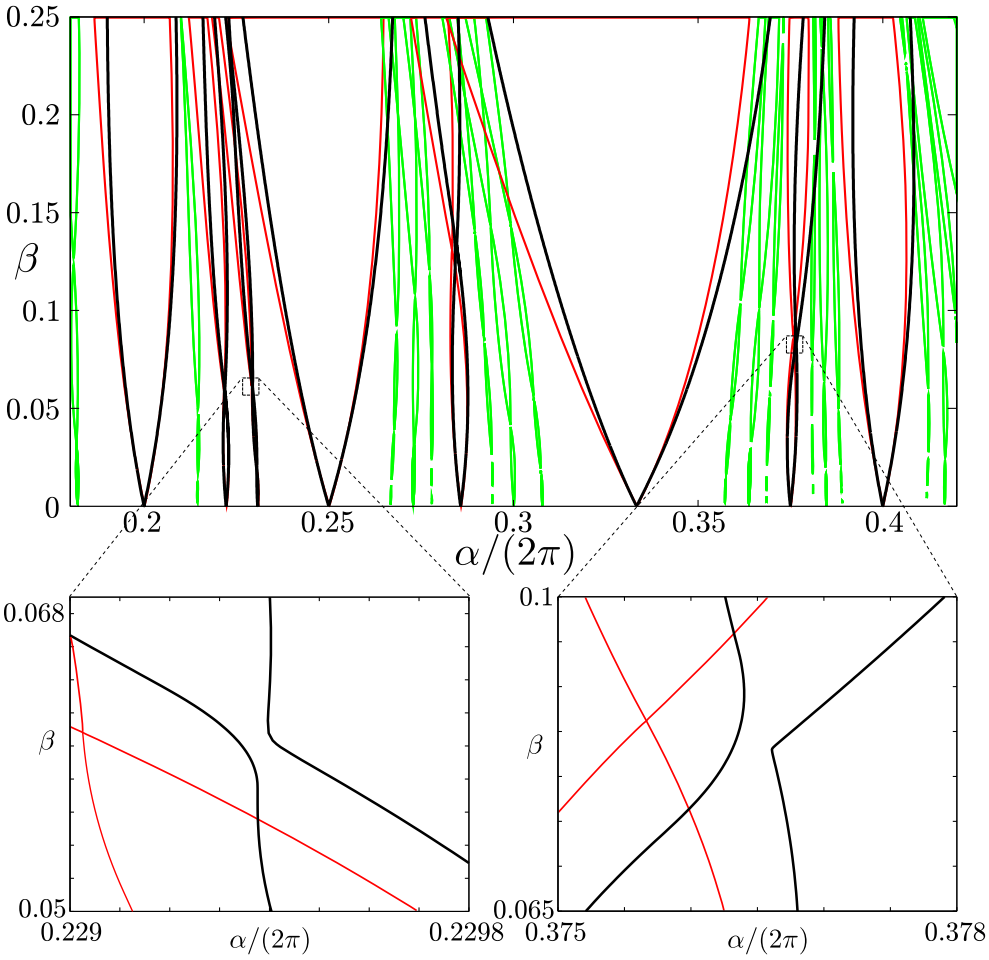

FIG. 7. *Comparison between the (black) saddle-node bifurcation curves for the smoothed vector field* (4.1) *and the border-collision bifurcation curves (red and green) for the piecewise-smooth normal form* (2.2). *Enlargements in the neighborhood of double border-collision points are shown in panels (b) and (c).*

where

$$J_\epsilon = J + \begin{pmatrix} 0 & 0 \\ 0 & \epsilon \end{pmatrix}.$$

(Note that the order of rotation and projection is as in [39], but this does not affect the geometry of the Arnol′d tongues at all.) The parameter ϵ controls the invertibility of (4.2). For fixed $C > 0$ and $\epsilon > 0$ large enough the map (4.2) is a diffeomorphism, but for small $\epsilon \geq 0$ it is only an endomorphism, that is, the map is not invertible.

The map (4.2) is non-invertible if there are points $\mathbf{y} \in \mathbb{R}^2$ for which the determinant of the Jacobian vanishes. After some algebra, we find that this happens when

$$1 + e^\nu + \nu + \epsilon + \epsilon\, e^{-\nu} - \nu\,\epsilon = 0, \tag{4.3}$$

where $\nu = 2C\,(1 - y_2)$. This equation has a minimum at $\nu = \log \epsilon$, which substituted

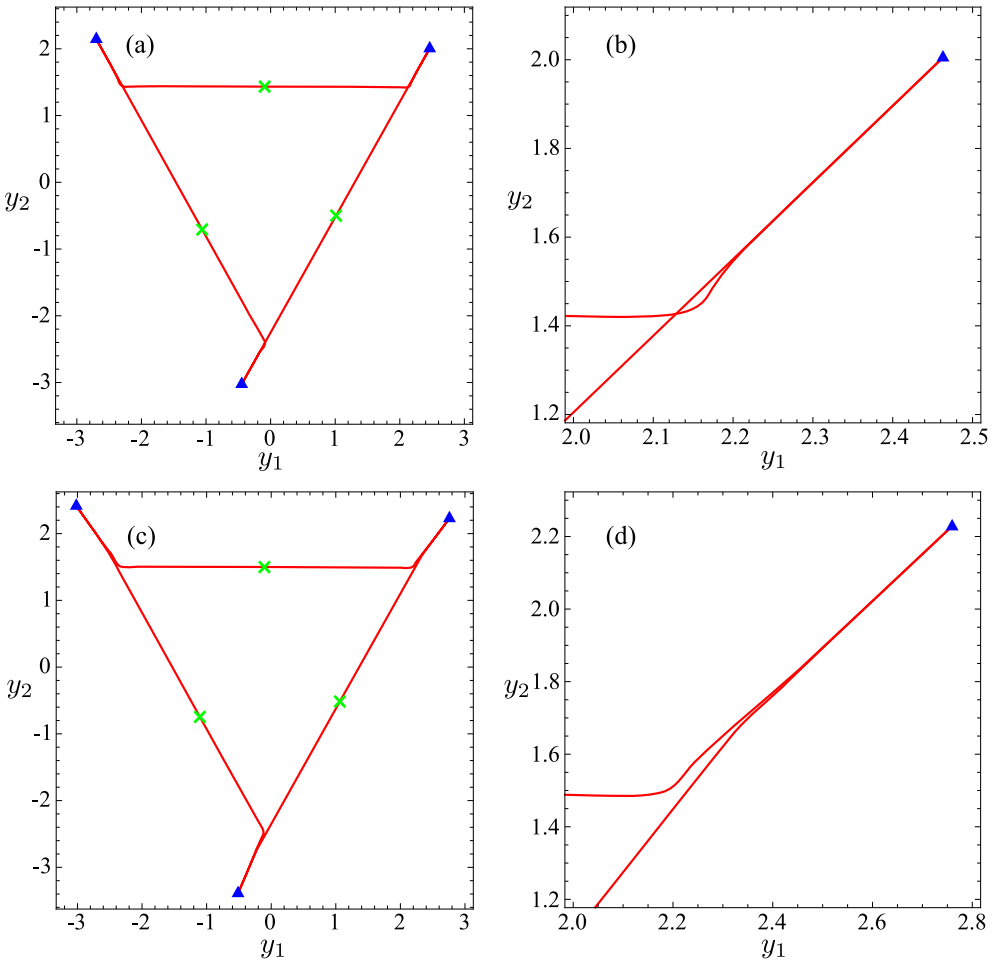

FIG. 8. *Phase portraits for* $\alpha = 0.333492 \times 2\pi$ *and* $\beta = 0.12$ *in the smoothed non-invertible map* (4.2) *with* $\epsilon = 0$ *in panels (a) and (b) and* $\epsilon = 0.090776 \approx \bar{\epsilon}$ *in panels (c) and (d). Shown are stable (blue triangles) and saddle (green crosses) periodic orbits of period three together with the one-dimensional unstable manifold (red) of the saddle that connects the two periodic orbits. The enlargements in panels (b) and (d) illustrate self-intersections of the manifold for* $\epsilon < \bar{\epsilon}$ *that go away as soon as the map becomes invertible* ($\epsilon > \bar{\epsilon}$).

back into (4.3) gives

$$2 + 2\epsilon + \log \epsilon - \epsilon \log \epsilon = 0.$$

Hence, the invertibility of the map does not depend on the smoothing parameter C. We find that there is a unique $\bar{\epsilon} \approx 0.090776$ so that the map (4.2) is a diffeomorphism for $\epsilon > \bar{\epsilon}$. Throughout this section, we use $C = 10$ and $\gamma = \beta/\alpha$.

Let us first investigate the effect of the parameter ϵ by considering the point $(\alpha, \beta) = (0.333492 \times 2\pi, 0.12)$, which lies well inside the 1/3 Arnol′d tongue. For the normal form (2.2) the values correspond to a system that has a three-sided minimal polygon $\mathcal{P}_f$ with 1/3 side ordering. The stable period-three orbit is located outside the polygon formed by the three intersection points of $\mathcal{P}_f$. Hence, we expect that a pair of stable and saddle period-three orbits exists and the unstable manifold of

the saddle periodic orbit forms a connection between the two period-three orbits that is similar to a three-sided polygon on $\mathcal{P}_f$. This heteroclinic cycle is not necessarily smooth, that is, the periodic orbits do not reside on a smooth invariant torus; see also [23]. Figure 8 shows the period-three orbits and the unstable manifolds for the endomorphism with $\epsilon = 0$ (top row) and at the critical boundary $\epsilon = 0.090776 \approx \bar{\epsilon}$ (bottom row). The stable periodic orbit is marked with blue triangles and the saddle periodic orbit with green crosses; the unstable manifold is red. Panels (a) and (c) show the entire heteroclinic cycle and panels (b) and (d) show an enlargment near the top-right point of the stable periodic orbit (blue triangles). Two branches of the unstable manifold (red) go to this point and since they approach the point from the same side, the closed curve is not a normally hyperbolic invariant manifold. In fact, the two branches intersect, a feature that can only happen for unstable manifolds in non-invertible systems [14]. If we take $\epsilon = \bar{\epsilon}$ at the boundary of invertibility the unstable manifold is tangent to itself; see Figs. 8(c) and (d). The manifolds form a topological circle as soon as $\epsilon > \bar{\epsilon}$, but the connection does not form a smooth torus.

Let us now consider the Arnol′d tongues of the smoothed map (4.2) and compare them with those for the normal form (2.2). We computed the boundaries of the tongues as fold bifurcation of periodic orbits in the continuation package AUTO [13] using $\epsilon = 0$. The result is shown in Fig. 9(a). As before, the saddle-node bifurcation curves are black and the corresponding border-collision curves are red; the other border-collision curves are green. At first glance, the agreement between the two maps is very good, because we hardly see any red. Of course, one can expect that a direct smoothing of the normal form leads to a better agreement than the Poincaré map of the smoothed vector field. However, there are discrepancies in the neighborhood of the double border-collision points. The typical unfolding that we would expect is inspired by studies in the context of quasi-periodically forced systems [31]. Locally each sausage transforms into a curve with a cusp point a little away from the border-collision point, such that a region with two coexisting pairs of stable and saddle periodic orbits is created, that is, the Arnol′d tongue can be viewed as two tongues that overlap.

The typical scenario that we find is shown in the enlargement in Fig. 9(b), which illustrates a slightly more complicated case. The part of the (red) Arnol′d tongue below the double border-collision point has transformed into a (black) cusped curve with a cusp near $(\alpha, \beta) = (0.283213 \times 2\pi, 0.1317)$. The (red) part above the double border-collision, however, has transformed into a (black) curve with three cusps creating regions with two and thee coexisting pairs of stable and saddle periodic orbits. Such unfoldings correspond to swallowtail singularities and are typical in smooth systems [2]; they have been studied extensively in the context of quasi-periodically forced systems [31]. Figure 9(c) shows a slightly different unfolding, where the swallowtail forms part of the tongue boundary. Rather than a "top-bottom" split of the tongue boundaries, the boundaries split "left-right" and the right boundary has two cusp points such that again an overlapping region is created with two coexisting pairs of stable and saddle periodic orbits.

We find that the Arnol′d tongues do not change qualitatively for $\epsilon > \bar{\epsilon}$, except that more cases occur where the double border-collision points unfold as in Figs. 7(b) and (c). Figure 10 shows several continuations of branches of periodic orbits along cross-sections with β fixed for $\epsilon = 0$. The vertical axis is the AUTO L_2-norm of the periodic orbit. The black lines are the saddle-node bifurcation curves that match those shown in Figs. 9(b) and (c). Each panel shows four cross-sections with β increasing

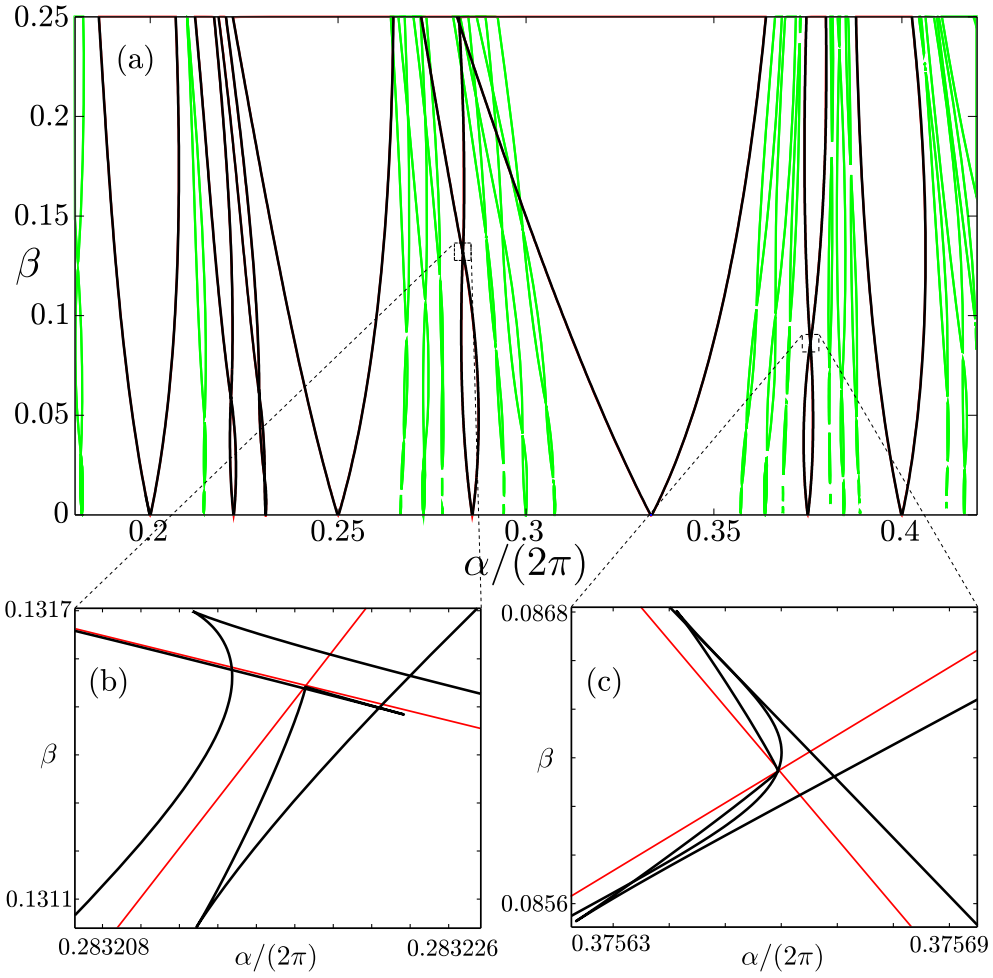

FIG. 9. *Comparison between the (black) saddle-node bifurcation curves for the smoothed non-invertible map* (4.2) *with* $\epsilon = 0$ *and the border-collision bifurcation curves (red and green) for the piecewise-smooth normal form* (2.2). *Enlargements in the neighborhood of double border-collision points are shown in panels (b) and (c).*

from green to red.

Figure 10(a) corresponds to Fig. 9(b). The first (green) cross-section shows a pair of stable and saddle periodic orbits born in a saddle-node bifurcation on the right in the picture (for large α). The fold point lies on a curve that forms the bottom part of the Arnol′d tongues and has a cusp at $\beta \approx 0.1317$. There is a second fold point on this same curve on the other side of the cusp point. These two saddle-node bifurcations mark the tongue boundary at this β-value. The two additional fold points create a region with another coexisting pair of stable and saddle periodic orbits. The yellow cross-section is for a slightly larger value of β and the situation is topologically the same. For a slightly larger β-value we encounter a cusp point and an additional two fold points are created; the blue cross-section contains a small range of α for which there are three coexisting pairs of stable and saddle periodic orbits. This region ends at the next cusp bifurcation that corresponds to the point with the excessive dip

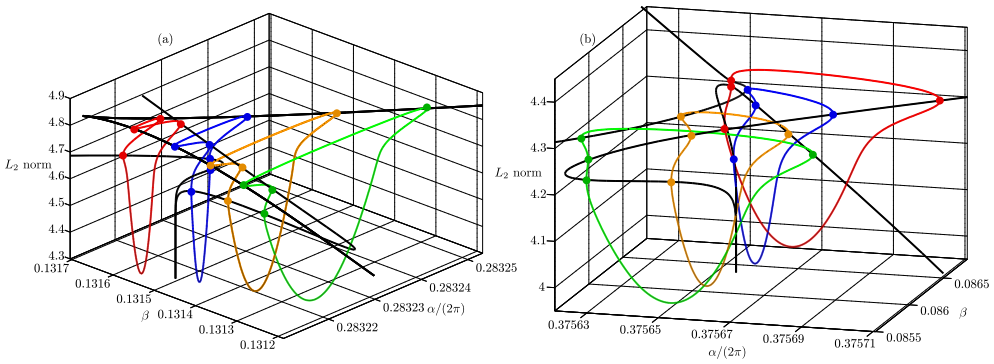

FIG. 10. *Continuation of the branch of periodic orbits through several horizontal (β constant) cross-sections of two Arnol′d tongues of the smoothed map (4.2) with $\epsilon = 0$. The parameter β is increasing from green, yellow, blue, to red. The black lines are saddle-node bifurcation curves that mark the tongue boundaries; panels (a) and (b) match the projections shown in Figs. 9(b) and (c), respectively.*

in L_2-norm. The red curve shows again a case with only two coexisting pairs, but compared to the first green curve it is the other pair of saddle-node bifurcations that mark the boundary of the Arnol′d tongue.

Figure 10(b) corresponds to Fig. 9(c). The left boundary of the Arnol′d tongue enters and exits through the plane with α constant on the left, running from the top left corner in the back plane with β constant to (somewhat) top left on the front. The other tongue boundary comes up from the bottom plane and creates three cusp points before leaving through the right side of the image. Here, there are always at most two coexisting pairs of stable and saddle periodic orbits. As in Fig. 10(a), the first green cross-section has four fold points with the left-most and right-most points forming the tongue boundary. The yellow cross-section is topologically equivalent in the sense that all fold points are still on the same curves on the same sides of the cusp points. The next blue cross-section shows how the right fold point that was inside the tongue takes over as the right tongue boundary, which is shown more clearly for the last red cross-section. In contrast to Fig. 10(a), there are only two coexisting pairs of stable and saddle periodic orbits throughout the transition, but the two fold points that play the role of tongue boundaries change more frequently and in a different manner.

5. Conclusions. We studied the formation of Arnol′d tongues at a grazing-sliding bifurcation of an unstable focus-type periodic orbit of a Filippov system. This setting is motivated by the example of a piecewise-smooth friction oscillator. Based on the equations for the friction oscillator, we derived a normal form in [39] in a neighborhood of the grazing-sliding bifurcation that describes the behavior on a Poincaré section transverse to the unstable periodic orbit as well as the switching surface. The dynamics on the section can be expressed in terms of a piecewise-linear map that includes the dynamics induced by sliding. As we showed in [39], the normal form has an attracting invariant set that resides on what we call the minimal polygon that consists of the switching line $\mathcal{K}_0$ and its first $q-1$ forward iterates; the minimal polygon then has q sides. We showed in this paper that the normal form gives rise to pairs of stable and saddle periodic orbits on the minimal polygon that are organized by Arnol′d tongues. We analyze the Arnol′d tongues in the (α, β)-parameter plane.

The boundaries of the Arnol′d tongues are border-collision bifurcations that open up for $\beta = 0$ at rational values $\frac{\alpha}{2\pi} = \frac{p}{q}$ of the ratio between the intrinsic frequency of the system and the forcing frequency. Except for the strong resonances $1/2$, $1/3$ and $1/4$, the Arnol′d tongues close up again at double border-collision bifurcation points, forming a string of sausages. Inside the first sausage, the phase-locked orbits contain one and two sliding segments (stick-phases of the friction oscillator), respectively. For $\beta > 0$ small enough and $-1 < \gamma < 1$, the periodic orbit with two sliding segments is stable and the periodic orbit with one sliding segment is of saddle type. Inside the second sausage, the orbit with two sliding segments coexists with a periodic orbit that has three sliding segments; and so on. In principle, the periodic orbit with the most sliding segments is stable and the other of saddle type, but as β increases, additional bifurcations may occur that change the stability of these orbits. The parameter space is divided into regions bounded by side-removal curves at which the number of sides of the minimal polygon changes. We showed that a double-border collision takes place each time when an Arnol′d tongue crosses a side-removal curve.

The organization of the Arnol′d tongues in a neighborhood of a grazing-sliding bifurcation is very similar to the organization of the tongues in a neighborhood of an ordinary grazing bifurcation in a Filippov system without sliding [36, 37, 46, 47]. However, the presence of a sliding region gives rise to a projection term in the normal form that renders it non-invertible. We used this property to show that an attracting invariant set resides on the minimal polygon that necessarily contains the switching line $\mathcal{K}_0$. We also expressed the dynamics on the minimal polygon in terms of an induced map defined on $\mathcal{K}_0$. The periodic orbits generated by the induced map are automatically admissible solutions of the normal form. Furthermore, the induced map allows for the formulation of implicit equations that define the border-collision bifurcations that bound the Arnol′d tongues. We believe that the sliding region has the effect that double-border collision bifurcations, where the Arnol′d tongues close up, are structurally stable and not merely due to the absence of higher-order terms in the normal form.

We compared the structure of the Arnol′d tongues for the normal form with smoothed versions of the friction oscillator; we considered both the smoothing of the friction term in the vector field itself and the smoothing of the normal form. The closing of Arnol′d tongues is not structurally stable for smooth systems, so we expected that the double border-collision points would unfold. Their unfoldings are entirely in line with what was predicted in [2].

We found that the periodic orbits do not always reside on the actual polygon formed by the segments in between the vertices of the minimal polygon. That is, the dynamics on the minimal polygon is not always topologically equivalent to that of a circle map. For such cases, the smoothed normal form does not have a normally hyperbolic invariant torus, not even when the smoothed map is invertible; see Fig. 8. The location of the phase-locked orbits relative to the vertices of the minimal polygon may hold the key to what constitutes a normally hyperbolic invariant torus for a piecewise-smooth system. The periodic orbits lie inside the vertices for parameter values inside the first sausage of an Arnol′d tongue, as long as $\beta > 0$ is small. Furthermore, it seems that some points of the periodic orbit move to the other sides of the vertices as soon as the tongue crosses a side-removal curve. The precise nature of this phenomenon and the nature of normal hyperbolicity will be the topic of future research.

Acknowledgments. We would like to thank Carles Simó and Joaquim Puig for pointing out the similarities of our sausages with instability pockets in Hill's equations and for providing the references. We are also grateful for helpful discussions with John Guckenheimer and James Meiss. HMO gratefully acknowledges the support and hospitality of Cornell University, where part of this work was carried out.

REFERENCES

[1] V. I. Arnol′d, *Geometrical Methods in the Theory of Ordinary Differential Equations*, Springer-Verlag, Berlin/New York, 1983.

[2] H. W. Broer, M. Golubitsky, and G. Vegter, *The geometry of resonance tongues: a singularity theory approach*, Nonlinearity, 16(4) (2003), pp. 1511–1538.

[3] H. W. Broer and M. Levi, *Geometrical aspects of stability theory for Hill's equations*, Arch. Rational Mech. Anal., 131 (1995), pp. 225–240.

[4] H. W. Broer and C. Simó, *Resonance tongues in Hill's equations: a geometric approach*, J. Differential Equations, 166(2) (2000), pp. 290–327.

[5] H. W. Broer and G. Vegter, *Bifurcational aspeects of parametric resonance*, Dynamics Reports, New Series 1 (1992), pp. 1–51.

[6] M. E. Broucke, C. C. Pugh, and S. N. Simić, *Structural stability of piecewise smooth systems*, Computation and Applied Mathematics, 20(1-2) (2001), pp. 51–89.

[7] D. K. Campbell, R. Galeeva, C. Tresser, and D. J. Uherka, *Piecewise linear models for the quasiperiodic transition to chaos*, Chaos, 6 (1996), pp. 121–154.

[8] A. Chenciner, *Bifurcations de points fixes elliptiques, II. Orbites périodiques et ensembles de Cantor invariants*, Invent. Math., 80(1) (1985), pp. 81–106.

[9] G. Csernák and G. Stépán, *On the periodic response of a harmonically excited dry friction oscillator*, J. Sound Vibrat., 295 (2006), pp. 649–658.

[10] M. di Bernardo, C. J. Budd, A. R. Champneys, and P. Kowalczyk, *Bifurcation and Chaos in Piecewise-Smooth Dynamical Systems: Theory and Applications*, Springer-Verlag, Berlin, 2007.

[11] M. di Bernardo, M. I. Feigin, S. J. Hogan, and M. E. Homer, *Local analysis of C-bifurcations in n-dimensional piecewise-smooth dynamical systems*, Chaos, Solitons & Fractals, 10 (1999), pp. 1881–1908.

[12] M. di Bernardo, P. Kowalczyk, and A. B. Nordmark, *Bifurcations of dynamical systems with sliding: derivation of normal-form mappings*, Physica D, 170 (2002), pp. 175–205.

[13] E. J. Doedel, A. R. Champneys, T. F. Fairgrieve, Yu. A. Kuznetsov, B. Sandstede, and X. Wang, *AUTO97: Continuation and bifurcation software for ordinary differential equations (with HomCont)*, Concordia University, Montreal, Canada, 1997, `http://cmvl.cs.concordia.ca/`.

[14] J. P. England, B. Krauskopf, and H. M. Osinga, *Bifurcations of stable sets in noninvertible planar maps*, Internat. J. Bifur. Chaos Appl. Sci. Engrg., 15(3) (2005), pp. 891–904.

[15] J. Farey, *On a curious property of vulgar fractions*, Phil. Mag. J. London, 47 (1816), pp. 385–386.

[16] B. Feeny and F. C. Moon, *Chaos in a forced dry friction oscillator: experiments and numerical modelling*, J. Sound Vibrat., 170 (1994), pp. 303–323.

[17] A. F. Filippov, *Differential Equations with Discontinuous Right-Hand Sides*, Kluwer Academic, Dordrecht, 1988.

[18] U. Galvanetto, *Unusual chaotic attractors in nonsmooth dynamic systems*, Internat. J. Bifur. Chaos Appl. Sci. Engrg., 15(12) (2005), pp. 4081–4086.

[19] L. Goldberg and C. Tresser, *Rotation orbits and the Farey tree*, Ergod. Thy. & Dynam. Sys., 16 (1996), pp. 1011–1029.

[20] F. Hofbauer and G. Keller, *Quadratic maps without asymptotic measure*, Commun. Math. Phys., 127(2) (1990), pp. 319–337.

[21] M. R. Jeffrey and A. Colombo, *The two-fold singularity of discontinuous vector fields*, SIAM J. Applied Dynamical Systems (in press).

[22] G. Keller and M. St. Pierre, *Topological and measurable dynamics of Lorenz maps*, in Ergodic Theory, Analysis, and Efficient Simulation of Dynamical Systems, B. Fiedler, ed., Springer-Verlag, Berlin, 1992, pp. 333-361.

[23] B. Krauskopf and H. M. Osinga, *Investigating torus bifurcations in the forced Van der Pol oscillator*, in Numerical Methods for Bifurcation Problems and Large-Scale Dynamical Systems, E. J. Doedel and L. S. Tuckerman, eds., IMA Volumes in Mathematics and its

Applications 119, Springer-Verlag, New York, 2000, pp. 199-208.
[24] Yu. A. Kuznetsov, *Elements of Applied Bifurcation Theory*, Springer-Verlag, New York, 2004.
[25] Yu. A. Kuznetsov, S. Rinaldi, and A. Gragnani, *One-parameter bifurcations in planar Filippov systems*, Internat. J. Bifur. Chaos Appl. Sci. Engrg., 13(8) (2003), pp. 2157–2188.
[26] R. P. McGehee and B. B. Peckham, *Resonance surfaces for forced oscillators*, Experiment. Math., 3(3) (1994), pp. 221–244.
[27] R. P. McGehee and B. B. Peckham, *Arnold flames and resonance surface folds*, Internat. J. Bifur. Chaos Appl. Sci. Engrg., 6(2) (1996), pp. 315–336.
[28] A. B. Nordmark, *Non-periodic motion caused by grazing incidence in an impact oscillator*, J. Sound Vibrat., 145 (1991), pp. 279–297.
[29] J. Nussbaum and A. Ruina, *A two degree-of-freedom earthquake model with static/dynamic friction*, Pure and Applied Geophysics, 125 (1987), pp. 629–656.
[30] H. E. Nusse and J. A. Yorke, *Border-collision bifurcations including "period two to period three" for piecewise smooth systems*, Physica D, 57(1-2) (1992), pp. 39–57
[31] H. M. Osinga, J. Wiersig, P. A. Glendinning, and U. Feudel, *Multistability and nonsmooth bifurcations in the quasiperiodically forced circle map*, Internat. J. Bifur. Chaos Appl. Sci. Engrg., 11(12) (2001), pp. 3085–3105.
[32] S. Östlund, D. Rand, J. Sethna, and E. Siggia, *Universal properties of the transition from quasi-periodicity to chaos in dissipative systems*, Physica D, 8(3) (1983), pp. 303–342
[33] K. Popp and P. Stelter, *Stick-slip vibration and chaos*, Phil. Trans. R. Soc. Lond. A, 332 (1990), pp. 89–105.
[34] F. Schilder, H. M. Osinga, and W. Vogt, *Continuation of quasiperiodic invariant tori*, SIAM J. Applied Dynamical Systems, 4(3) (2005), pp. 459–488.
[35] F. Schilder and B. B. Peckham, *Computing Arnol′d tongue scenarios*, J. Computational Physics, 220(2) (2006), pp. 932–951.
[36] D. J. W. Simpson and J. D. Meiss, *Neimark-sacker bifurcations in planar, piecewise-smooth, continuous maps*, SIAM J. Applied Dynamical Systems, 7(3) (2008), pp. 795–824.
[37] D. J. W. Simpson and J. D. Meiss, *Shrinking point bifurcations of resonance tongues for piecewise-smooth, continuous maps*, Nonlinearity, 22(5) (2000), pp. 1123–1144.
[38] R. Szalai, *PDDE-CONT: A continuation and bifurcation software for delay-differential equations*, Budapest University of Technolgy and Economics, Budapest, Hungary, 2005, `http://seis.bris.ac.uk/~rs1909/pdde/`.
[39] R. Szalai and H. M. Osinga, *Invariant polygons in systems with grazing-sliding*, Chaos, 18 (2008), p. 023121.
[40] F. Takens, *Forced oscillations and bifurcations*, in Applications of Global Analysis I, Communications of the Mathematical Institute Rijksuniversiteit Utrecht 3 (1974), pp. 1–59; reproduced in Global Analysis of Dynamical Systems, H. W. Broer, B. Krauskopf, and G. Vegter, eds., Institute of Physics Publishing, Bristol, 2001, pp. 1–61.
[41] M. A. Teixeira, *Generic bifurcation of sliding vector fields* J. Mathematical Analysis and Applications, 176(2) (1993), pp. 436–457.
[42] J. Llibre, P. R. da Silva, and M. A. Teixeira, *Regularization of discontinuous vector fields on $\mathbb{R}^3$ via singular perturbation* J. Dynamics and Differential Equations, 19(2) (2007), pp. 309–331.
[43] J. Llibre, P. R. da Silva, and M. A. Teixeira, *Study of singularities in nonsmooth dynamical systems via singular perturbation* SIAM J. Applied Dynamical Systems, 8(1) (2009), pp. 508–526.
[44] V. I. Utkin, *Sliding Modes in Control and Optimization*, Springer-Verlag, New York, 1992.
[45] W. Yang and B. Hao, *How the Arnold tongues become sausages in a piecewise linear circle map*, Communications in Theoretical Physics, 8 (1987), pp. 1–15.
[46] Z. T. Zhusubaliyev and E. Mosekilde, *Bifurcations and Chaos in Piecewise-smooth Dynamical Systems*, Nonlinear Science Series A Vol. 44, World Scientific, River Edge, 2003.
[47] Z. T. Zhusubaliyev, E. Mosekilde, S. Maity, S. Mohanan, and S. Banerjee, *Border collision route to quasiperiodicity: numerical investigation and experimental confirmation*, Chaos, 16 (2006), p. 023122/11.
[48] Z. T. Zhusubaliyev, E. A. Soukhoterin, and E. Mosekilde, *Border-collision bifurcations and chaotic oscillations in a piecewise-smooth dynamical system*, Internat. J. Bifur. Chaos Appl. Sci. Engrg., 11(12) (2001), pp. 2977–3001.